Universitätsklinikum Hamburg-Eppendorf

Hochschule für Angewandte Wissenschaften Hamburg
Hamburg University of Applied Sciences
Fakultät Life Sciences

Hochschule für angewandte Wissenschaften Hamburg
Fakultät für Life Science

Department Biotechnologie

Bachelorthesis

Construction of Fluorescent Sensor Molecules for the Detection of Local Concentrations of Extracellular ATP

zur Erlangung des akademischen Grades
Bachelor of Science

Autorin: Sonja Katharina Klose [redacted]

Abgabedatum: August 9, 2021

1. Gutachter: Prof. Dr. Claus-Dieter Wacker
2. Gutachter: Prof. Dr. med. Friedrich Haag

Contents

List of Figures

List of Tables

Ab antibody

Abs Antibodies

ADO adenosine

ADP adenosine diphosphate

AMP adenosine monophosphate

ATeam Adenosine 5'-Triphosphate indicator based on Epsilon subunit for Analytical Measurements

ATP Adenosine triphosphate

BCA Bicinchoninic acid

BSA bovine serum albumin

Ca^{2+} calcium ions

CD Cluster of differentiation

CFP Cyan fluorescent protein

CO_2 carbon dioxide

cpSFGFP circular permuted superfolded GFP

ddH_2O double-distilled water

diH_2O deionized water

DMSO Dimethyl sulfoxide

DNA Deoxyribonucleic acid

FACS fluorescence-activated cell sorting

FCS Fetal calf serum

FPLC fast protein liquid chromatography

FRET Förster resonance energy transfer

FSC forward scatter

GFP green fluorescent protein

GTP guanosine triphosphate

HRP horseradish peroxidase

Ig immunoglobulin

IPTG Isopropyl-β-D-thiogalactoside

LDS loading dye solution

mfi median fluorescence intensity

Mg^{2+} magnesium ions

Nb nanobody

Nbs nanobodies

NEDP1 NEDD8-specific protease 1

Ni-TED nickel-tris-carboxymethyl ethylene diamine

PAGE polyacrylamide gel electrophoresis

PBS phosphate buffered saline

PBMCs peripheral blood mononuclear cells

PFA Paraformaldehyde

PVDF Polyvinylidene fluoride

RPMI Roswell Park Memorial Institute

rpm revolutions per minute

RT room temperature

SA streptavidin

SDS sodium dodecyl sulfate

SOC Super optimal broth with catabolite repression

SRA sample reducing agent

SSC side scatter

TAE tris base-acetic acid-EDTA buffer

UDP uridine 5'-diphosphate

UTP uridine 5'-triphosphate

UV ultraviolet

YFP yellow fluorescent protein

1 Aim of this work

Adenosine triphosphate (ATP) is known as the universal energy carrier of living cells. It plays not only an important role in the cell's energy metabolism, it also has relevance as a paracrine and autocrine signalling molecule. The release of ATP is involved in many biological processes such as the regulation of the immune system and inflammatory responses. Human cells constantly release small amounts of ATP. It can be released by damaged cells, transported via channels and carriers, and via vesicular release. Biological, chemical or mechanical stress such as sheer forces, inflammatory reactions, osmotic stress or a change in the culture medium can significantly increase the amount of released ATP. Extracellularly, the response to ATP is determined by a variety of membrane-bound receptors that are activated by nucleotide binding. ATP binding regulates various physiological functions. It is involved in many signalling processes and its role is not yet fully understood. The ability to measure or even monitor ATP concentrations intra- and extracellularly could help to broaden and deepen the understanding of these processes. The luciferin-luciferase system is the most commonly used assay to measure ATP concentrations. However, only global concentration changes are detected. To measure local ATP concentration, small molecule sensors are needed.
The goals of this thesis were to construct fluorescent sensor molecules for the detection of local ATP concentrations, to bring them close to the cell surface and to prove their function as ATP sensors. Three ATP sensors were investigated in this thesis. To construct the ATP sensor molecules and to evaluate their function, the following tasks had to be accomplished:

- Cloning of DNA sequence into a bacterial expression plasmid and validation of sequence
- Transformation of bacteria for protein expression
- Cells lysis and protein purification
- Protein modification (His tag cleavage, labelling with dye)
- Evaluation of sensor function in cell free systems and bound to cells

2 Introduction

Adenosine triphosphate (ATP) is known as an universal intracellular energy storage and carrier medium that occurs naturally in every cell of the body [1]. It is synthesized in various ways - including glycolysis and the citric acid cycle [2]. Its stored energy is released when the phosphoanhydride bonds are hydrolyzed (see Fig. 1) [3].

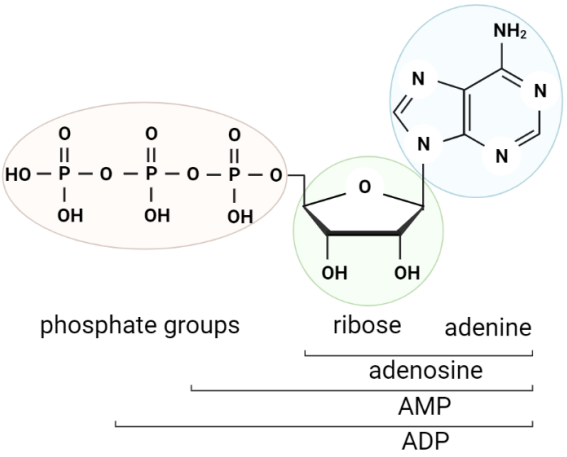

Figure 1 Structure of adenosine triphosphate and its metabolites. Adenosine triphosphate (ATP) consists of an adenine residue, the sugar ribose and three phosphate residues. The bonds of the three phosphate residues are very high-energy chemical bonds. If these bonds are hydrolytically cleaved by enzymes, adenosine diphosphate (ADP) or adenosine monophosphate (AMP) is formed. Energy is released in the process. Created with BioRender.com.

2.1 ATP as signaling molecule

Besides its role in energy metabolism, Burnstock *et al.* described ATP as a second messenger molecule for intra- and extracellular signal transduction [4] which targets among others two receptor families P1 and P2 receptors [5]. Burnstock *et al.* also introduced the term "purinergic" signaling in 1972. In general, P1 receptors are more sensitive to adenosine (ADO) and AMP, whereas P2 receptors are more sensitive to ADP and ATP [5]. Activation of those receptors leads to pro- or anti-inflammatory signaling cascades. The release of ATP and its metabolites is involved in many biological processes such as the regulation of the immune system and inflammatory reactions. Furthermore, ATP has an important function as a neurotransmitter [1] and is involved in cell-cell communication [6].

2.1.1 ATP release and metabolism

Intracellularly, ATP is needed for countless processes such as protein synthesis, muscle contraction and enzyme regulation [2]. The ATP concentration inside the cell is in the

millimolar range, and significantly higher than outside the cell [7]. Basal concentrations of intracellular ATP range from 1 mM to 10 mM [8] [9], whereas the extracellular concentration is around 10 nM [10] [11] [12]. The pericellular concentration can be a little higher in the "pericellular halo", which is maintained via continuous release of ATP [13]. Human cells constantly release small amounts of ATP (see Fig. 2). It can be

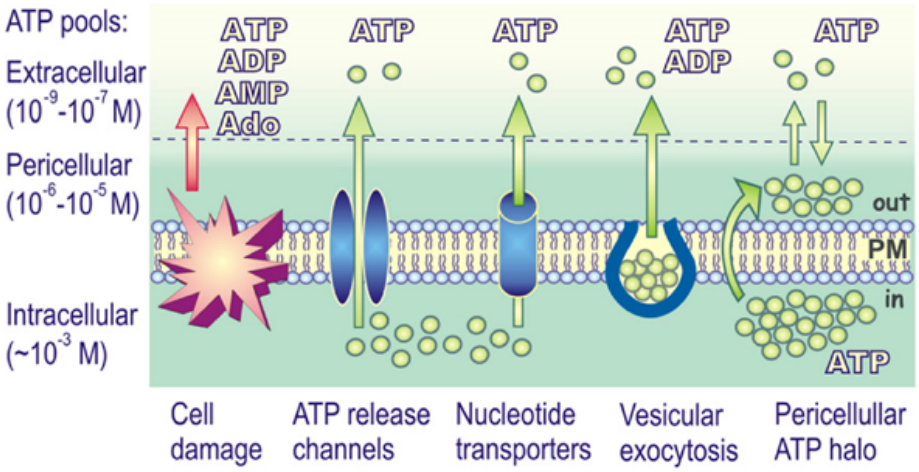

Figure 2 Release of endogenous nucleotides. ATP enters the extracellular space by various mechanisms, which include transport via channels, transport proteins and vesicular exocytosis. Resting cells passively release ATP, creating the "pericellular halo". If the cell is damaged, nucleotides are released from inside the cell. Figure according to Yegutkin (2008) [14].

released by damaged cells, transported via channels and carriers, and via vesicular release [15]. Biological, chemical or mechanical stress such as sheer forces, inflammatory reactions, osmotic stress or a change in the culture medium can significantly increase the amount of released ATP [6]. Extracellularly, the response to ATP is determined by a variety of membrane-bound receptors that are activated by nucleotide binding. ATP binding regulates various physiological functions [1]. For example, released nucleotides from apoptotic cells serve as signal molecules to recruit phagocytes to eliminate the dying cell [16]. Besides, ATP can serve as a signal molecule for cells releasing the nucleotide (autocrine) and their neighboring cells (paracrine) (see Fig. 3). Outside the cell, ATP is degraded by various surface molecules such as the ectoenzymes CD39 and CD73 [17], which results in low ATP concentrations despite constant ATP release, and a steady state is reached [18].

2.1.2 Purinergic signaling

Due to its short half-life of only a few seconds and its dispersion by regional blood or fluid flow, signaling events of ATP are limited to a narrow radius [19][20]. As a result, released nucleotides and their metabolites function as local paracrine or autocrine signaling molecules by activating purinergic receptors such as P1 and P2 receptors (see

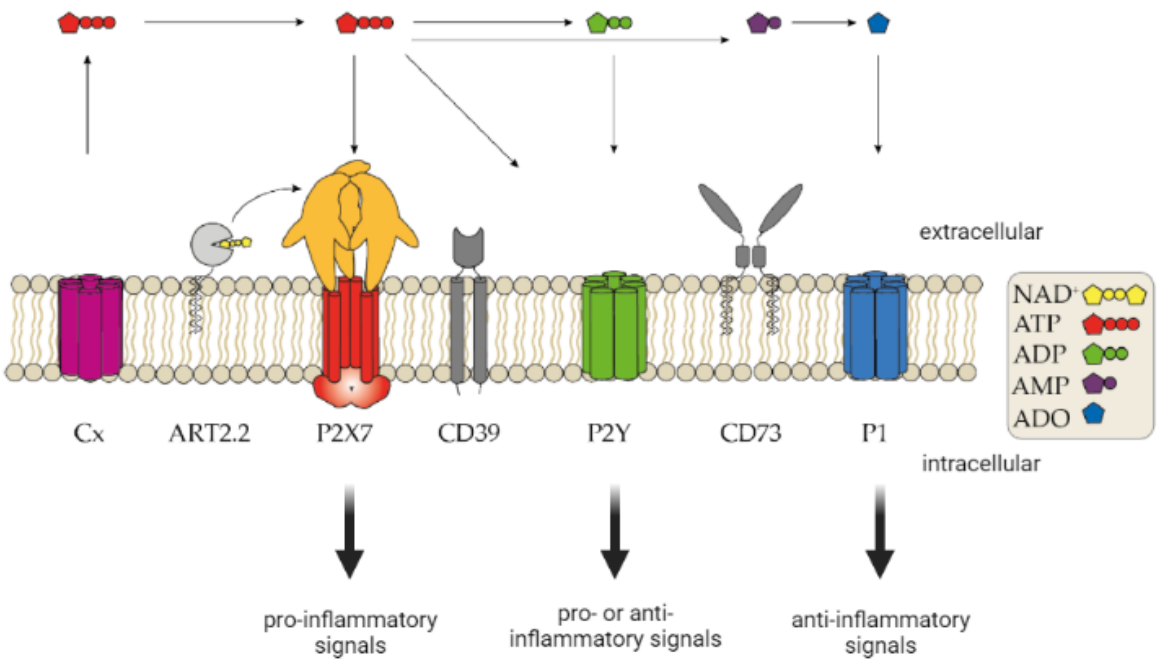

Figure 3 Schematic overview of receptors, channels and enzymes taking part in the purinergic signalling cascade. ATP is released into the extracellular space by various mechanisms such as transport via channels, transport proteins and vesicular exocytosis. Binding to receptors causes inflammation (P2X and P2Y) or triggers anti-inflammatory signals (P2Y and P1). ATP is hydrolyzed to ADP or AMP via ectoenzymes such as CD39 and further cleaved by CD73 to ADO which activates the P1 receptor. Image modified from Kaschubowski (2020) [21].

Fig. 3)[6]. Virtually all cell types express P2 receptors but their responses to extracellular nucleotides are diverse, depending on nucleotide concentration, presence/absence of other mediators in the microenvironment, extent of stimulation and other factors [22].

When released as a result of stress or tissue damage, ATP functions as a danger signal and mediates pro-inflammatory responses such as chemotaxis, release of pro-inflammatory cytokines and chemokines and stimulation of effector T cell functions. Di Virgilio *et al.* (2009) and Lofti *et al.* (2018) showed that ATP can also promote immunosuppressive activities [23][24].

Purinergic receptors

Purinergic receptors can be divided in two families (P1 and P2) with subfamilies and subtypes. Until now, four P1 receptors (A_1, A_{2A}, A_{2B} and A_3) were characterized. These receptors either activate (A_{2A} and A_{2B}) or inhibit (A1 and A3) the function of the enzyme adenylate cyclase and have specific agonists and antagonists for each subtype [22] [25]. The P2 receptor family contains two subfamilies P2X and P2Y.

P2X receptors are ligand-gated ion channels with seven family members ($P2X_{1\text{-}7}$). P2Y receptors are G protein-coupled receptors with eight known human subtypes [25].
ADO is a purine nucleoside and a metabolite of ATP that plays an important role in the body and can bind extracellularly to P1 receptors, which are expressed on the cell surface of various immune cells of the innate immune response (neutrophils, macrophages, mast cells, dendritic cells and natural killer cells). Depending on which receptor ADO binds to, the innate immune response is coordinated during various inflammatory conditions (e.g. acute inflammatory responses such as sepsis and chronic ones (such as asthma or cancer)) [26].
The A_{2A} receptors appear to be most significant for adenosine-mediated immune regulation, as they trigger a wide range of anti-inflammatory but also inflammatory responses of the immune system [27]. Regulatory mechanisms are crucial to limit uncontrolled tissue damage by activated immune cells. When extracellular ADO accumulates in inflamed regions, further tissue damage is prevented by suppressing the activity of immune cells through binding of ADO to the A_{2A} receptor. ADO functions as an agonist, which means that binding to the receptor causes a conformational change that activates the receptor. The binding of an agonist is intended to suppress the immune response [2].

2.2 ATP measurement and sensors

As described in 2.1, ATP is an important extracellular signaling molecule and plays a role in different physiological and pathological processes, including inflammation, neurotransmission, cancer development and as indicator for apoptosis[24] [28]. In order to investigate the mechanisms of these processes, an understanding of extracellular ATP dynamics is highly important. Therefore, different approaches to measure ATP were developed over the last 50 years, including bioluminescence assay methods using firefly luciferase [29], electrochemical methods including voltammetry [30], enzyme-coupled electrode techniques [31] [32], cell-based electrophysiological techniques [33] [34], and whole cell-based fluorescence assay methods using calcium ions (Ca^{2+}) indicator [35] [36].
The luciferin-luciferase reaction [29] is the most commonly used approach to measure extracellular ATP. Luciferase is found in different insects commonly known as fireflies. Upon ATP binding to the enzyme, the substrate luciferin is oxidised, resulting in a bioluminescence signal that can be detected by luminometers. This technique is very sensitive. Low ATP concentrations down to high femtomolar concentrations can be detected without interference of other nucleotides (e.g. uridine 5'-triphosphate (UTP), uridine 5'-diphosphate (UDP), ADP). Another advantage is the fast response time of milliseconds. However, the system is very susceptible to interference. The enzyme has its optimum at room temperature and pH 7.8. It needs magnesium ions (Mg^{2+}) and

high salt concentrations. Among other factors, various anions inhibit the luciferase. Another problem is that bulk measurements of extracellular ATP do not reflect the "true" ATP concentration in the environment of the cell. The concentration is more precise when the luciferase is attached to the cell membrane, but the method still lacks the temporal and spatial resolution for measurement on the microscope [15]. Another way to measure ATP concentration is to detect it indirectly through Ca^{2+} increase. Therefore, biosensor cells expressing P2X or P2Y receptors are used. They are co-cultured with cells of interest, which release ATP after certain stimulation. This in turn results in P2X- or P2Y-mediated calcium influx in the biosensor cells and can be detected by a calcium indicator such as FuraRed [21]. ATP concentrations that are sufficient to activate the P2 receptor, ranging from higher nanomolar to lower millimolar ATP concentrations, can be detected with this method [15]. An alternative approach are genetically encoded ATP sensors including Förster resonance energy transfer (FRET)-based sensors such as ATeam (Adenosine 5'-Triphosphate indicator based on Epsilon subunit for Analytical Measurements) [37], and ratiometric sensors such as QUEEN [38]. Their high selectivity for ATP compared to other nucleotides (ADP, guanosine triphosphate (GTP) and UTP) is an advantage, as well as their easy handling. They do not need such specific conditions as e.g., luciferase. Sensors like ATeam allow specific temporal and spatial measurement of ATP levels [37].

Förster resonance energy transfer (FRET) and FRET-based ATP sensors

Förster resonance energy transfer (FRET) is a nonradiative energy transfer between an excited donor fluorophore and a suitable acceptor molecule through long-range dipole dipole coupling, first described by Theodor Förster in 1948 [39]. This photophysical process is distance-dependent and occurs only in close range (1 10 nm) without collision (< 1 nm) or dominant photon emission of the donor (> 10 nm). If two molecules in close proximity are fluorochromes, the changes due to FRET, are reflected in fluorescence intensity, fluorescence lifetime and quantum efficiency. Due to its sensitivity to small distance changes, FRET is a suitable method to study dynamic molecular events such as conformational changes in macromolecules. Using two fluorescent probes for FRET, the efficiency depends on the distance and relative orientation of the dipoles as well as that the emission spectrum of the donor and the absorption spectrum of the acceptor must overlap [39] [40].

Genetically encoded FRET sensors form single polypeptide chains consisting of two fluorescent proteins and a recognition domain. As a result of ligand binding (e.g. ATP), the recognition domain undergoes a conformational change that alters the distance and relative orientation between the FRET pair. Depending on the design of the sensor, the ligand binding can lead to an increase or a decrease of the FRET. Both effects can be used as a readout signal by fluorescence detectors [40]. A broad range of

fluorescent proteins is available, especially due to engineering of the green fluorescent protein (GFP) and its derivatives. For instance, cyan fluorescent protein (CFP) and yellow fluorescent protein (YFP) are a widely used donor-acceptor pair [39].
Imamura *et al.* developed a genetically encoded FRET sensor for ATP that was named ATeam containing the CFP - YFP FRET pair. It is fused to the ϵ-subunit of bacterial F0F1-ATP synthase from *Bacillus sp.* PS3, which binds ATP specifically and undergoes a conformational change upon binding (see Fig. 4). It does not hydrolyse ATP and

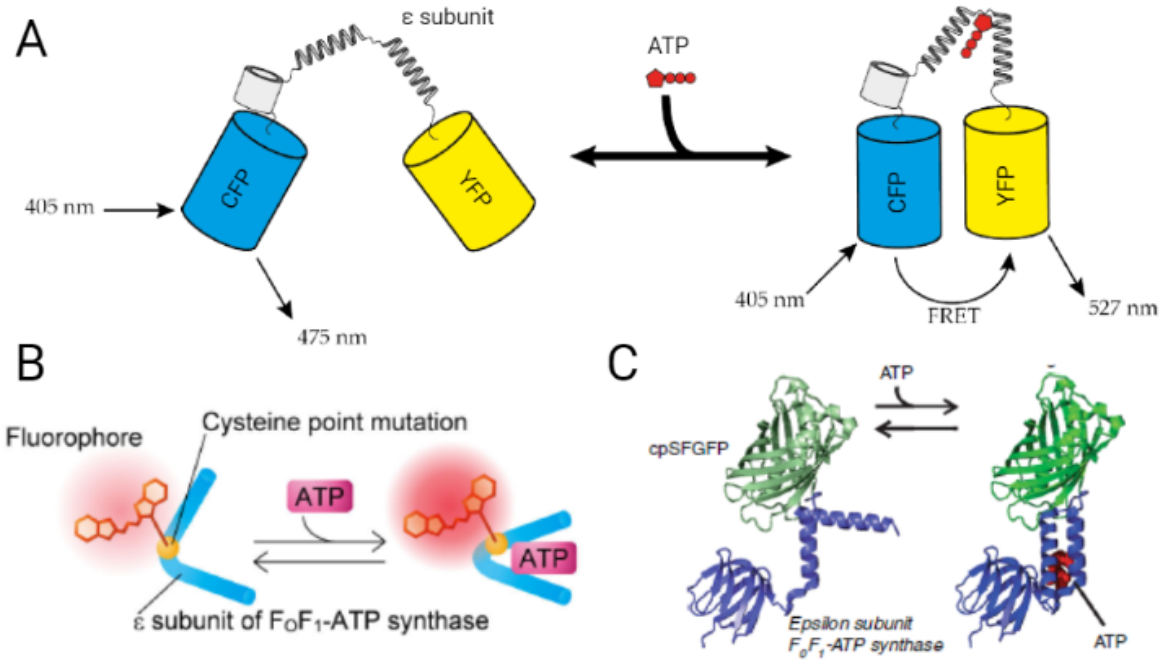

Figure 4 Design of ATP sensors based on ϵ-subunit of bacterial F0F1-ATP synthase. (A) The FRET-based ATeam sensor has the ϵ-subunit of bacterial F0F1-ATP synthase as ATP binding domain flanked by the GFP derivatives CFP and YFP. ATP binding induced conformational change of the domain alters the distance between CFP and YFP. In absence of ATP, fluorescence emission from the donor CFP at 475 nm is primary detected while YFP acceptor emission at 527 nm dominates in presence of ATP. (B) ATPOS, the ϵ-subunit of the F0F1-ATPase from *Bacillus* PS3 labeled with Cy3, shows an increase in fluorescence intensity when ATP is bound. It is excited at 550 nm and emits at 570 nm. Fluorescence can be detected with PE channel in flow cytometry or fluorescence microscopy. (C) ATP binding to the ϵ-subunit of the F0F1-ATPase from *Bacillus* PS3 induces a conformational change leading to a brighter signal of the coupled GFP of the TP1170_HHM1.1 sensor. Its peak excitation is at 490 nm and peak emission at 512 nm. Image modified from (A) Kaschubowski (2020)[21], (B) Kitajima *et al.* (2020)[41] and (C) Lobas *et al.* (2019)[42].[1]

is almost insensitive to other nucleotides and ATP metabolites. As a negative control Imamura *et al.* designed a version of ATeam named Bs_RRKK which does not bind ATP. For this purpose, they replaced the two arginine residues of the ATP binding domain from *Bacillus subtilis* (Bs), which interact with the α and β phosphates of ATP, with lysine residues, which do not interact with ATP [37].

In this study two small molecule single wavelength sensors based on FRET-based ATP sensors were used. Both ATP sensors have the ϵ-subunit of the F0F1-ATPase from *Bacillus* PS3 as ATP binding domain. The two sensors are described in the following.

2.2.1 Single wavelength sensor TP1170_HHM1.1

One of the ATP sensors used in this work is a single-wavelength genetically encoded fluorescent sensor (iATPSnFR) based on the GFP according to Lobas *et al.* (2019). To construct this sensor, Lobas *et al.* inserted circular permuted superfolded GFP (cpSFGFP) into the ϵ-subunit of the F0F1-ATPase from *Bacillus* PS3. This subunit undergoes a pronounced conformational change when ATP is bound, which results in an increase of cpSFGFP fluorescence (see Fig. 4). The sensor developed by Lobas *et al.*, named iATPSnFR$^{1.1}$, is sensitive to ATP in the micromolar range but less well expressed by cells than a second sensor they developed. The sensor showed no significant affinity to the metabolites of ATP. The protein displayed a fluorescence spectrum with peak excitation at 490 nm and peak emission at 512 nm [42].
The ATP sensor, TP1170_HHM1.1, constructed and used in this thesis, is based on the sensor variant iATPSnFr$^{1.1}$ (called HHM1.1) of Lobas *et al.* (2019). To be able to bring the sensor close to cell surface, the molecule was constructed as a fusion protein containing HHM1.1, combined with TP1170 nanobody.

Conventional and heavy chain antibodies

Antibodies (Abs), also called immunoglobulin (Ig), are used by the immune system to identify and neutralize pathogens. They exist in two forms, membrane bound on the surface of B cells, working as antigen receptors, or as secreted antibodies. Those unbound antibodies neutralize toxins through binding, prevent pathogens from entering the cell and spreading and eliminate microbes. All antibodies share the same basic structure - two identical heavy chains and two identical light chains, which are connected via disulfide bonds (see Fig. 5). Both chain types contain constant regions, which mediate effector functions, and variable regions which recognize and bind antigens. They are highly variable and bind to their specific antigen.
Human Abs are divided into isotypes according to differences in the constant region of the heavy chains. Different isotypes or subclasses have different functions in immune responses due to the binding of the heavy chain constant region to different cells or proteins. They are divided into IgA (IgA1 and IgA2), IgD, IgE, IgG (IgG1, IgG2, IgG3 and IgG4) and IgM. In mice, which are often used in the study of immune responses, the IgG isotype is divided into the IgG1, IgG2a, IgG2b, and IgG3 subclasses. In this work, mouse IgG1 and IgG2 subtypes are used.
Light chains are also divided into two isotypes, called κ and λ, based on their constant

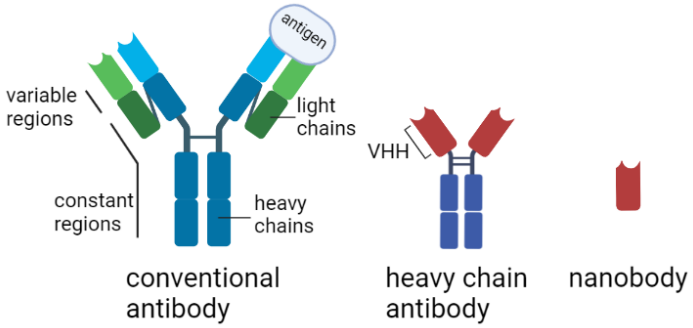

Figure 5 Structure of conventional and heavy chain antibody. Conventional antibody (Ab) such as IgG are found in all vertebrates and consist of two identical light chains and two identical heavy chains. The two heavy chains as well as the light chain and its heavy chain are covalently bound by disulphide bonds which are indicated here by black lines. The heavy chain antibody has two heavy chains with only two domains and one variable domain VHH (variable domains of the heavy chain of heavy chain antibodies) each. This variable domain is also named nanobody due to is small size and its ability to recognize and bind antigens. Created with BioRender.com.

region. So far no differences in function are described [43]. Camelids like llamas and alpacas express Abs, which lack light chains (see Fig. 5) in addition to conventional Abs. These so-called heavy chain Abs recognize antigens by one single variable domain, which can be produced as a recombinant protein in bacteria, yeast, or plant cells. Due to the small size of the domain, this protein is named nanobody or single domain antibody [44].

The ability to produce some nanobodies (Nbs) (such as TP1170, which is used in this work) recombinantly in bacteria is a major advantage for research over conventional Abs, which are produced in immunized animals [45]. Nbs have only one domain and no post-translational modifications so they can be easily cloned into bacterial or mammalian vectors and produced recombinantly on a large scale with little effort [46]. With a molecular weight of about 15 kDa, they are the smallest antibody fragments (see Fig. 5), that recognize and bind antigens. Their small size allows them to bind to epitopes that are difficult to access for conventional Abs [47]. In 2018, Pleiner *et al.* described several nanobody (Nb) constructs against mouse and rabbit IgG. One of those Nbs is TP1170 which recognizes mouse κ-chains, which are part of about 99 % of all mouse Abs [45]. Since TP1170 binds to any κ-chain mouse Abs, it is used in the context of this work as a way of bringing the coupled ATP sensor molecule close to the cell surface to detect local ATP concentrations.

2.2.2 Small-molecule sensor ATPOS

Kitajima *et al.* (2020) recently described a high-sensitivity ATP sensor named ATPOS (ATP optical sensor) for extracellular imaging in the nanomolar and micromolar range. This sensor also uses the ϵ-subunit of the F0F1-ATPase from *Bacillus* PS3, which is

the same ATP binding domain as the FRET-based ATP sensors originally described by Imamura *et al.* (2009). ATPOS is designed as a hybrid-type fluorescent ATP sensor composed of the ATP binding protein and a small-molecule fluorescent dye. The dye can be conjugated via a cysteine-reactive maleimide group to a single cysteine. Kitajima *et al.* initially tested four promising small-molecule fluorescent dyes, Oregon Green, Alexa Fluor 488, Cy3 and SiR650. The conjugate exhibiting the largest fluorescence response at a wide range of ATP concentrations was the Cy3-labeled construct. They named the binding protein labeled with Cy3 ATPOS.
ATPOS shows an increase in fluorescence in the presence of ATP (see Fig. 4). It also shows a high affinity for ATP but almost no sensitivity to ATP metabolites, such as AMP or ADO, or different nucleotides like GTP and UTP. According to Kitajima *et al.* ATPOS is insensitive to pH changes between pH 6.0 and 8.5 in the presence or absence of ATP [41].

3 Materials

3.1 Antibodies and nanobodies

Table 1 Antibodies/nanobodies used for FACS and microscopy

ANTIGEN	FLUORESCENCE	CLONE	MANUFACTURER
ALFA tag	PO		Nolte Lab, UKE
Biotin-CD3	unconjugated	OKT3	BioLegend
Biotin-cmyc	unconjugated	9E10	BioLegend
CD3	APC	SK7	BD Biosciences
cmyc	unconjugated	9E10	BioLegend
Mouse	PO		GE Healthcare
mouse IgG	APC	none	MolProb
mouse IgG1	BV421		
Strep tag	PO	none	iba

3.2 Bacterial strains

Table 2 Bacterial strains

NAME	TYPE	MANUFACTURER
E. coli BL21(DE3)pLysS	competent cells	Novagen
E. coli XL.1 blue	competent cells	Stratagene

3.3 Enzymes

Table 3 Enzymes

NAME	MANUFACTURER	NUMBER
Antarctic Phosphatase	New England Biolabs	M0289S
Hind III	New England Biolabs	R0104S
Kas I	New England Biolabs	R0544S
NEDD8-specific protease 1 (NEDP1)	Haag Lab, UKE	
Not I	New England Biolabs	R0189S
T4 DNA Ligase	New England Biolabs	M0202L

3.4 Buffers and solutions

Table 4 Buffers and solutions

NAME	COMPOSITION
LB agar	40 g/l LB agar diH_2O
Lysing Buffer	5 mL BugBuster 50 μL AEBSF (100 mM) 0.5 μL Benzonase
RPMI complete	500 mL RPMI 10 % (v/v) FCS 1 % (v/v) sodium pyruvate (100 mM) 1 % (v/v) L-glutamine (200 mM)
Blot buffer	100 mL transfer buffer 200 mL methanol 2 mL antioxidant ad aqua dest ->2l
SOC medium	0.5 % (m/v) yeast extract 2.0 % (m/v) trypton 10 mM NaCl 2.5 mM KCl 10 mM Ca_2 10 mM $MgSO_4$ 20 mM D(+)-glucose diH_2O
TBS Buffer	137 mM NaCl 2.7 mM KCl 25 mM TRIS diH_2O, pH 7.6

3.5 Chemicals and reagents

Table 5 Chemicals and reagents

CHEMICAL	MANUFACTURER	NUMBER
2x YT medium	Sigma-Aldrich	Y2377-250G
Adenosine triphosphate (ATP)	Sigma-Aldrich	A2383-1G
AEBSF	Sigma-Aldrich	532586
Antarctic Phosphatase Reaction buffer, 10x	New England Biolabs	B0289S
Aqua ad	Braun	0082479E
Benzonase	Merck	E1014-5KU
bovine serum albumin (BSA)	Sigma-Aldrich	9048-46-8
Bugbuster	Merck	70921
Calcium chloride ($CaCl_2$)	Carl Roth	A119.1
Centrifugal Filters, Amicon Ultra 30 kDa	Merck	UFC8033024
CL-XposureTM Film	Thermo Scientific	34089
Cy3-maleimide, 1 mg	Lumiprobe	11080
D-(+)-Glucose	Sigma-Aldrich	G8270-1KG
dimethyl sulfoxide (DMSO)	Sigma-Aldrich	D2650-100ML
Ethanol	Carl Roth	K928.4
fetal calf serum (FCS)	Gibco	16250078
GeneRuler, 1 kb	Thermo Scientific	SM0314
GeneRuler, 100 bp	Thermo Scientific	SM0243
Glycerol		
InstantBlue	expedeon	
isopropyl-β-D-thiogalactoside (IPTG)	Roche	10724815001
Kanamycin	Carl Roth	T832.2
LB Agar	Carl Roth	X969.2
LE Agarose	Biozym	652324
L-Glutamin, 200mM	Gibco	25030081
Methanol	Carl Roth	82.3
Milk powder	Carl Roth	T145.2
NEB Buffer 2.1, 10x	New England Biolabs	B7204S
NuPAGE Antioxidant	Invitrogen	NP0005
NuPAGE loading dye solution (LDS)	Invitrogen	NP0007
NuPAGE MES SDS Running Buffer, 20x	Invitrogen	NP0002
NuPAGE Sample Reducing Agent, 10x	Invitrogen	NP0009
NuPage Transfere Buffer, 20x	Invitrogen	NP0006
Penicillin, 10000U=mL	Gibco	15140122
Phosphate buffered saline (PBS-/-)	Gibco	14190-094

Poly-l-lysine 30 - 70 kDa, lyophilized	Sigma-Aldrich	P7280-5MG
Precision Plus Protein Kaleidoscope Standards	Bio-rad	161-0375
Roti-Safe Gel Stain	Carl Roth	3865.1
RPMI medium 1640	Gibco	21875-034
Sharp Pre-Stained Protein Standard	Novex	LC5800
Sodium pyruvate, 100 mM	Gibco	11360-039
Streptavidin_APC	MolProb	S-21375
Streptavidin_BV421		
Stripping Buffer	Thermo Scientific	21059
Supermarker	Nolte Lab, UKE	
T4 DNA Ligase Buffer, 10x	New England Biolabs	B0202A
TAE, 50x	Invitrogen	24710030
Transparent Streptavidin Beads, 5 μm	PolyAn	10521005
Tris-HCl	Carl Roth	9090.3
Trypan blue	Carl Roth	1680.1
Tween20	Fisher Scientific	BP337-100

3.6 Cell lines

Table 6 Cell lines

CELL LINE	CELL TYPE	ORIGIN	GROWTH
Jurkat	human cell lymphoma	Guse Lab, UKE	suspension cells
PBMCs	peripheral blood mononuclear cells	Haag Lab, UKE	suspension cells

3.7 Kits

Table 7 Kits

NAME	NUMBER	MANUFACTURER
BCA Protein Assay Kit	23225	Thermo Scientific
ECL-Kit	RPN2106	GE Healthcare
LS-Columns	130-042-401	Miltenyi Biotec
Nucelospin gel and PCR clean-up	750.609.250	Macherey-Nagel
Protino Ni-TED 150 Packed Columns	745 100.10	Macherey-Nagel
QIAprep Spin Miniprep Kit (250)	27106	QIAGEN

3.8 Laboratory equipment

Table 8 Laborytory equipment

NAME	TYPE	MANUFACTURER
Analytical balance	1412	Sartorius AG
Balance	Scout Pro	Ohaus
Biological Safety Cabinet	Herasafe KS12	Thermo Sientific
blotting chamber		invitrogen
Centrifuge	Heraeus Pico 17	Thermo Scientific
Centrifuge	Rotanta 460R	Hettich GmbH
Centrifuge	Sorvall RC-26+	DuPont
Counting chamber	Neubauer improved	Brand GmbH
Curix developer		AGFA
Flow cytometer	Canto II	Becton Dickinson
Freezer		Liebherr
Freezer	-20 °C	Liebherr
Freezer	4 °C	Liebherr
Gel electrophoresis chamber		Peqlab biotechnology
Gel electrophoresis chamber	Novex Mini Cell	invitrogen
Heat block		Eppendorf
Incubator		Sanyo
Incubator	Unitron	HT Infors
Incubator	Ecotron	HT Infors
Microscope	Axiovert 200M	Zeiss
Microscope	TCS SP8	Leica
Multichannel Finnpipette	5 - 50 μL	ThermoLabsystems
Multichannel Finnpipette	50 - 300 μL	ThermoLabsystems
Multilable counter	Victor	PerkinElmer
Nanodrop	2000c	Peqlab biotechnology
pH meter	MP220	Mettler toledo
Photometer		Implen
Pipette	10 μL	Eppendorf
Pipette	100 μL	Eppendorf
Pipette	1000 μL	Eppendorf
Pipette	2.5 μL	Eppendorf
Pipette	20 μL	Eppendorf
Pipette	200 μL	Eppendorf
Pipette Filler	accu-jet pro	Brand GmbH & Co KG
Plate reader	Infinite 200	TECAN

Power supply	250/2,5	Bio-Rad
Power supply	PowerPac 200	Bio-Rad
Roller mixer	SRT6	Stuart
Shaker		Medgenix Diagnostics
UV table	TI 1	Biometra
Vortex mixer		Heidolph
Water bath		Gesellschaft für Labortechnik
Transilluminator		peQlab

3.9 Plasmids

Table 9 Plasmids

INSERT	VECTOR
cmyc_alfa_ATPOS	pH14N8_TP1170_3C_HHM1.1_TEV_TwST
ATPOS_RRKK	pH14N8_cmyc_alfa_ATPOS
iATPSnFR1.1	pH14N8_TP1170_3C_TEV_TwST
iATPSnFR1.1_RRKK	pH14N8_TP1170_3C_HHM1.1_TEV_TwST

3.10 Consumables

Table 10 Consumables

DEVICES	MANUFACTURER	NUMBER
μ-Slide 8 well ibiTreat	ibidi GmbH	80826
96-well plate, flat	Thermo Scientific	167008
Amicon Ultra, 3 kDa cutoff	Sigma-Aldrich	UFC800324
Cryo-tube, 1.8 mL	Thermo Scientific	375418PK
Inoculation loop	Greiner bio-one	731170
NuPage 10% Bis-Tris-Gel	invitrogen	NPO342BOX
NuPage 12% Bis-Tris-Gel	invitrogen	NPO341BOX
Petri dish, 10 cm	Greiner bio-one	633180
Pipette tips, 10 μL	Sartsedt	70.1130.600
Pipette tips, 100 μL	Sartsedt	70.760.412
Pipette tips, 200 μL	Sartsedt	70.760.002
Pipette tips, 1000 μL	Sartsedt	70.760.100
Serological pipette, 1 mL	Sartsedt	86.1251.025
Serological pipette,10 mL	Sartsedt	86.1254.025
Serological pipette, 2 mL	Sartsedt	86.1252.025

Serological pipette, 25 mL	Falcon	356525
Serological pipette, 5 mL	Sartsedt	86.1253.025
Stericup, 150 mL	Millipore	S2GPU01RE
Tube, 0.2 mL	Sarstedt	72.737.002
Tube, 0.5 mL	Sarstedt	72.704.200
Tube, 1.5 mL	Sarstedt	72.706.200
Tube, 1.5 mL SafeSeal, brown	Sarstedt	72.706.200
Tube, 2 mL	Sarstedt	72.695.200
Tube, 5 mL	Greiner bio-one	1972337
Tube, 15 mL	Greiner bio-one	1970326
Tube, 50 mL	Greiner bio-one	1995152

3.11 Software

Table 11 Software

SOFTWARE	VERSION	MANUFACTURER
Excel	Office 2016	Microsoft
FACS	Diva 8.0	Becton Dickinson
Fiji	1.52t	Wayne Rasband (NIH)
FlowJo (Mac)	9.6	Becon Dickinson
FlowJo (Windows)	10.06.1	Becon Dickinson
Prism	8.4.3	GraphPad
Nanodrop 2000/2000C	1.2.	Peqlab
Snap Gene Viewer	5.0.7	GSL Biotech LLC
LaTeX TeXstudio	3.1.2	LaTeX Project Team

4 Methods

4.1 Methods in molecular biology

4.1.1 Restriction digestion of DNA

Restriction digestion process was used to precisely cleave a DNA fragment at a defined location using restriction enzymes. Restriction enzymes are highly specific tools cutting at a specific recognition sequence of DNA. These restriction endonucleases recognize specific DNA segments of 4 - 8 nucleotides (see Tab. 12) and cleave the phosphodiester bonds of two adjacent nucleotides. Hydrolysis at the phosphodiester ends results in

Table 12 Overview of restriction enzymes

Restriction enzymes	Cut Site
Hind III	5‘...A’AGCTT...3‘ 3‘...TTCGA’A...5‘
Kas I	5‘...G’GCGCC...3‘ 3‘...CCGCG’G...5‘
Not I	5‘...GC’GGCCGC...3‘ 3‘...CGCCGG’CG...5‘

the formation of so called "sticky ends" (see Fig. 6). The use of two different restriction enzymes at the respective ends of insert and plasmid backbone ensure that the insert is introduced into the vector in the desired orientation.

Parallel to each other, 4 μg insert and 3 μg vector were used in 1.5 mL Eppendorf microreaction tubes. To prepare the new constructs of insert and vector, the digest was prepared as described in Table 13 and incubated in the Thermocycler at 37 °C for 3 hours. Afterwards, the restriction enzymes were inactivated at the appropriate enzyme dependent temperature for 20 min.

Table 13 Overview digested DNA

1x NEB buffer 2.1	2 μl
DNA	x μL
enzyme 1	1 μL
enzyme 2	1 μL
ddH_2O	y μL
Total	20 μL

4.1.2 Dephosphorylation

To minimize the chance of religation without insert DNA, the vector DNA was dephosphorylated after restriction digest. The 20 μL vector DNA were incubated for 1 h

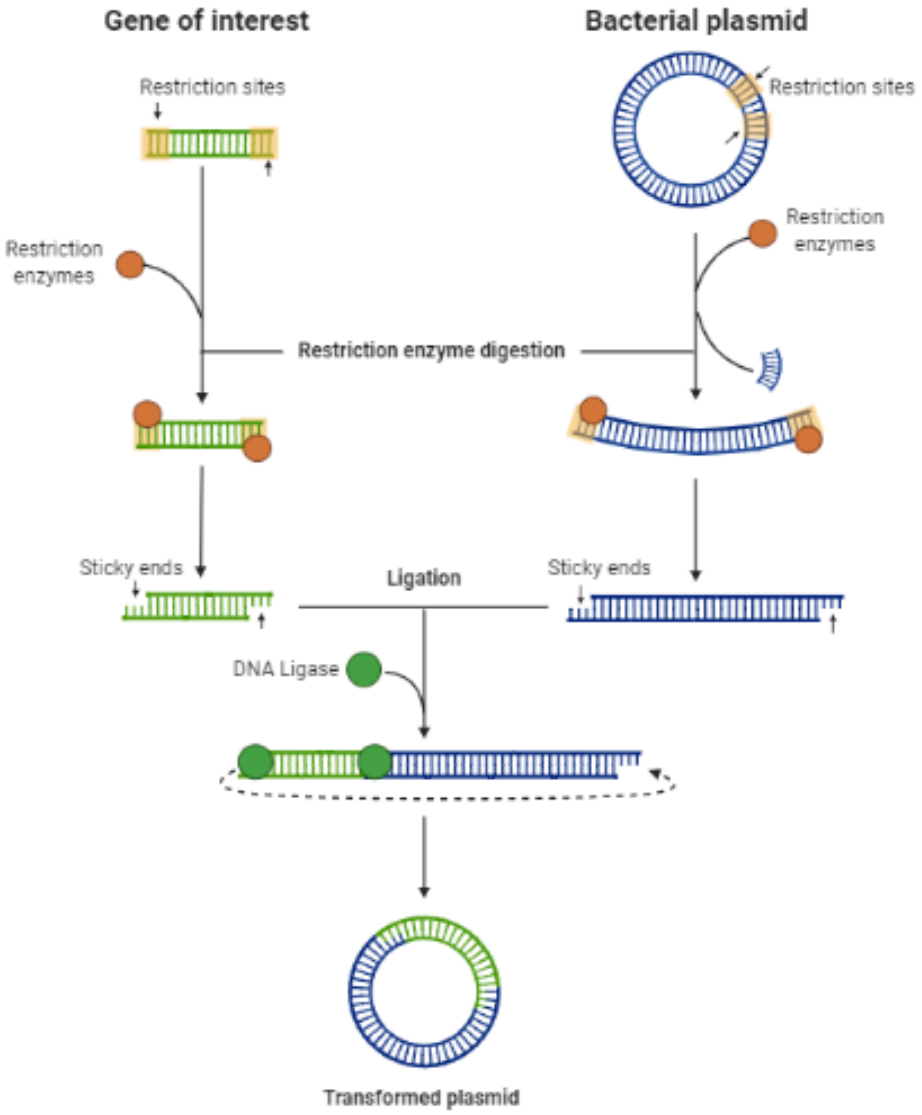

Figure 6 Schematic overview of restriction digestion and ligation. The gene of interest and the bacterial plasmid are both cut by the same highly specific restriction enzymes. To ensure that the insert is introduced into the vector in the desired orientation, two different restriction enzymes are used. The bacterial plasmids ring structure is now opened and a small number of nucleotides between the cutting sides is cut out. Hydrolysis at the phosphodiester ends results in the formation of so called "sticky ends" which allow the targeted linking of the DNA strands. DNA ligase links the fragments together and the ring is closed again. Adapted from “Restriction Anzymes Cloning”, by BioRender.com (2021) [48].

at 37 °C with 1 μL antarctic phosphatase, 3 μL of the antarctic phosphatase buffer and 6 μL water. Afterwards the enzyme was inactivated at 65 °C for 20 min.

4.1.3 Agarose gel electrophoresis

To purify, separate and identify DNA fragments, agarose gel electrophoresis was performed. For this purpose, digested DNA samples were mixed with 6x DNA Loading Dye and loaded onto a 1 % agarose gel in tris base-acetic acid-EDTA buffer (TAE).

Electrophoresis was performed for 40 - 60 min at 70 V (small gel) or 100 V (large gel). Roti-Safe GelStain was used to visualize the DNA under ultraviolet (UV) light. To extract DNA fragments from the agarose gel, visible bands were cut out on an UV transilluminator. The gel piece with the DNA of interest was transferred into a microcentrifuge tube. The NucleoSpin© Gel und PCR Clean-up Kit (Macherey-Nagel, Düren) was used to extract the deoxyribonucleic acid (DNA) according to manufacturer's specifications (see Fig. 7). Distilled water was used to elute DNA instead of the kit's elution buffer. The DNA concentration was determined using NanoDrop. Absorption at 260 nm (A260) was used to calculate the concentration. The ratio of A260/A280 was used for qualitative analysis of the nucleic acid solutions. A value between 1.8 and 2.0 indicated high purity.

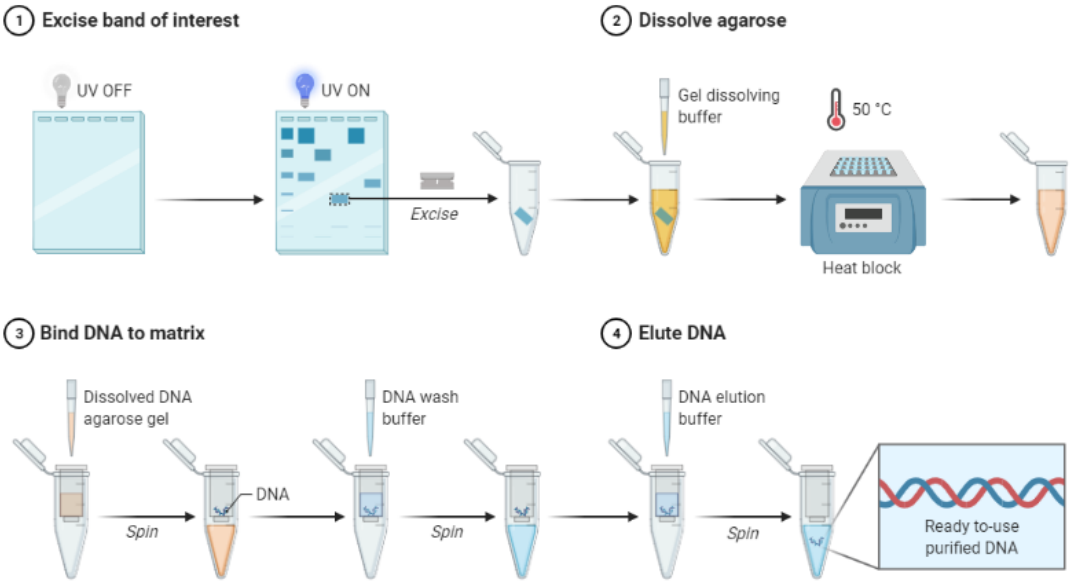

Figure 7 DNA gel extraction.(1) Under UV light, the visualised band of interest was separated from the gel and transferred to an 1.5 mL tube. (2) Double amount of gel dissolving buffer was added and then incubated at 50 °C for 5 - 10 min until the gel was completely dissolved. (3) The sample was loaded onto the column and centrifuged for 30 s at 11000 rpm. Flowthrough was discarded and the column was washed twice with DNA wash buffer. To make sure all ethanol containing wash buffer was removed from the column, it was centrifuged again for 1 min. (4) 20 μL water were added and incubated at room temperature for 1 min and centrifuged for 1 min afterwards. The flowthrough was loaded again onto the column, incubated, and centrifuged to elute the DNA completely. Adapted from "DNA Gel Extraction", by BioRender.com (2021) [48].

4.1.4 Ligation

To combine the vector DNA with the insert DNA, T4 DNA ligase was used to link the fragments. The T4 ligase connects the corresponding sticky ends to create the new

plasmid. For the ligation, 100 ng of vector DNA were used, the mass of insert was calculated using the following formula:

$$m_{\text{insert}} = \frac{bp_{\text{insert}}}{bp_{\text{vector}}} \cdot m_{\text{vector}} \cdot \frac{3}{1}$$

Vector and insert were incubated for 20 min at room temperature with 1 μL T4 DNA ligase, 1 μL of T4 ligase buffer and water if needed in a total reaction volume of 20 μL. A second reaction mix without insert DNA was used as control. This control is called religation.

4.1.5 Transformation

Bacteria were transformed to amplify plasmids of interest. For transformation, 50 μL competent *E. coli* XL-1 blue cells were thawed on ice, 4 μL ligation mixture were added and mixed by gentle swirling. The tubes were incubated on ice for 30 min and then placed in a water bath tempered to 42 °C for 30 s. After heat shock, the tubes were immediately incubated on ice for 2 min. Then 450 μL of pre-warmed SOC medium were added to the bacteria and incubated for one hour at 37 °C in a shaker at 220 rpm before being plated on LB agar containing kanamycin to select for transformed bacteria. The plates were incubated overnight at 37 °C. Bacteria without target plasmid do not have the antibiotic resistance gene and therefore cannot grow. Bacteria that were transformed with the vector without insert DNA should not grow either because the vector should not religate. Colonies on this plate would mean that the vector reconnected without the insert.

4.1.6 Isolation of plasmid DNA

To prepare plasmid DNA, a single colony of transformed XL1-blue was picked with a sterile pipettetip and transferred to 5 mL 2xYT medium for overnight culture at 37 °C and 180 rpm. The overnight culture was centrifuged for 10 min at 4000 rpm and 4 °C. All further steps were performed according to manufacturer's specifications from *QIAprep Spin Miniprep* Kit (Qiagen, Hilden)(see Fig. 8). Nanodrop was used to determine the concentration of nucleic acids in solution.

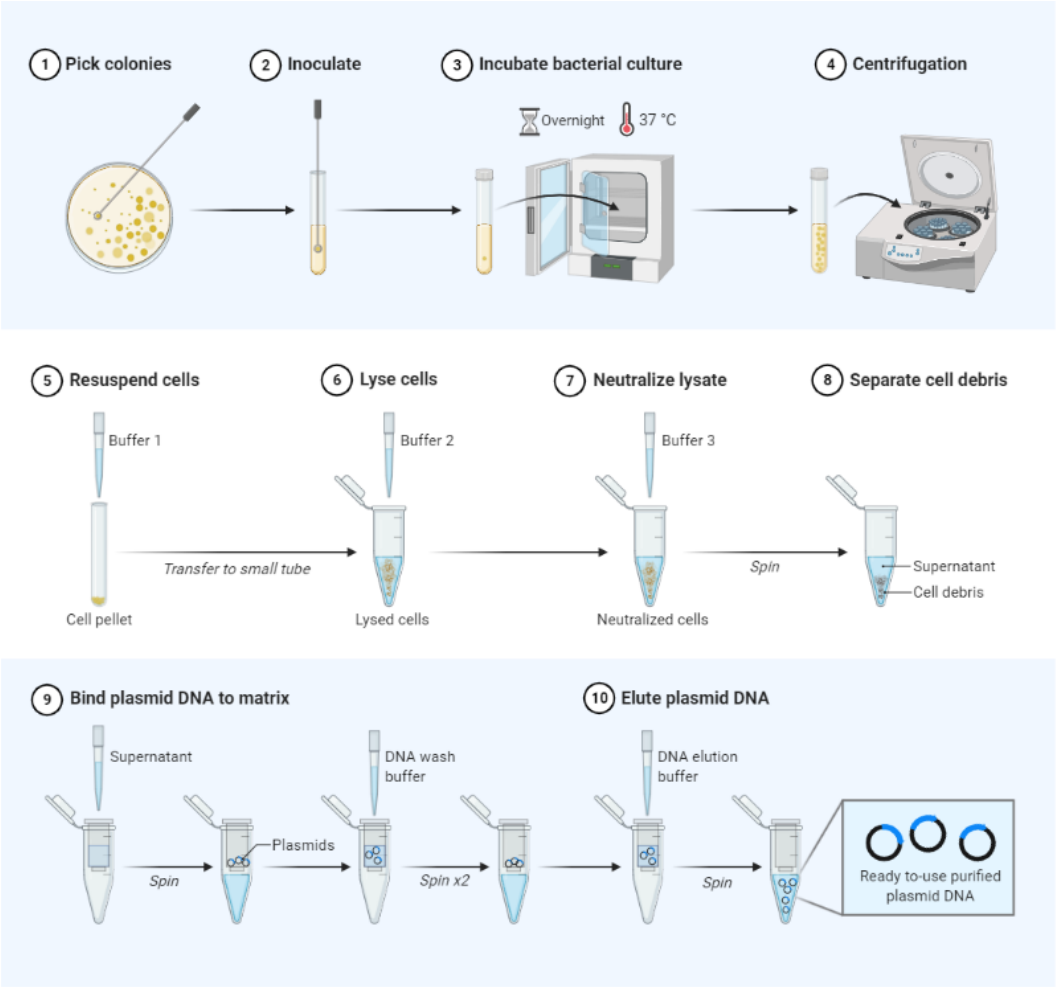

Figure 8 Workflow miniprep. (1) Four single colonies were picked and (2) used to inoculate 5 mL cultures, (3) which were incubated overnight at 37 °C at 220 rpm. (4) Bacterial cultures were centrifuged for 10 min at 4000 rpm and 4 °C. Supernatant was discarded. (5) The pellet was resuspended in 250 μL P1 buffer (+RNAse) and transferred to an 1.5 mL tube. (6) 250 μL buffer P2 were added, and the tube was inverted for four to six times. After 3 - 5 min incubation (7) 350 μL buffer N3 were added. The tube was inverted 4 - 6 times until a clear phase showed. (8) The cells were centrifuged for 10 min at 13.000 rpm to separate lysate and cell debris. (9) The supernatant was loaded onto the column and centrifuged for 30 s at 13.000 rpm. Flowthrough was discarded and 500 μL buffer PB were added. The plasmids were centrifuged for 30 s at 13.000 rpm. 750 μl buffer PE were loaded and centrifuged twice (30 s, 60 s) at 13.000 rpm. (10) The column was transferred to a fresh tube and incubated with 50 μL buffer EB for 1 min before centrifuged at 13.000 rpm for 1 min to elute the purified plasmid DNA. Adapted from "Plasmid Purification (Miniprep) Protocol", by BioRender.com (2021) [48].

4.1.7 DNA sequencing

To confirm that the cloning was successful and the insert was correctly inserted, constructs were sequenced by Eurofins Genomics using a kit purchased from the company. For this, plasmid DNA with a concentration between 50 ng/μL and 100 ng/μL was mixed with 2 μL of 10 μM primer solution and adjusted to a final volume of 17 μL with distilled water. The samples were sent back to Eurofins for Sanger sequencing.

Sequencing results are provided by the Eurofins genomics browser platform. The sequences were evaluated with the programs Snap Gene and Snap Gene Viewer and the websites expasy and multalign. To sequence the bacterial vectors (see 9), the primers NEDD8for (forward) and pQE80Lrev (reverse) were used.

4.2 Methods in protein chemistry and immunology

4.2.1 Flow cytometry

Flow cytometry was used to determine the characteristics of particles in a liquid stream. Each particle was individually passed and excited by a laser of suitable wavelength in order to analyze it separately. The flow cytometer (fluorescence-activated cell sorting (FACS)) can measure relative size (fetal calf serum (FCS)), granularity or complexity (side scatter (SSC)) and fluorescence intensity, providing information about cell type. The fluorescence intensity also provides information about expression level of antigens detected with fluorochrome conjugated antibodies.
When analyzed with the FlowJo program, the measurement results can be displayed as a histogram plot or as a dot plot. The histogram plots the frequency distribution - the signal intensity is plotted against the number of measured events. If the signal intensities of two different parameters are plotted against each other, a dot-plot diagram can be displayed, among others. In a dot plot diagram, individual populations are often easier to distinguish. By setting a gate, a population can be determined and analyzed in more detail.

4.2.2 SDS-PAGE

To seperate proteins by size via electrophoresis, sodium dodecyl sulfate (SDS) polyacrylamide gel electrophoresis (PAGE) was used. Molecular weight standard (SM) was applied in parallel to the samples to determine the protein size of the unknown sample. A 1x and a 4x concentrated marker was used to estimate protein amount after staining. Samples and markers were mixed 1:4 with LDS and 1:10 with SRA and denatured for 10 min at 70 °C in a heating block. Ready-cast 12 % Bis-Tris gels from invitrogen were used for this purpose and MES running buffer was added to the electrophoresis chamber. Gels were loaded with 20 μl per well. For western blot (see 4.2.3), 10 μL of kaleidoscope marker or 6 μL of pre-stained marker were added instead of SM. A voltage of 200 V was applied for 40 min to separate the samples. The gel was then used for western blot or stained with InstantBlue (Coomassie staining). For staining, the gel was incubated overnight in the staining solution on the laboratory shaker and decolorized in water for one hour the next day before scanning.

4.2.3 Western Blot

Polyvinylidene fluoride (PVDF) membrane was activated for 15 s in methanol and equilibrated in blot buffer for 10 min. Sponges and filter paper were also soaked in blot buffer and placed in the blot chamber. Blotting sandwich was built in the following order (bottom to top): 2x sponge, filter, gel (see 4.2.2), membrane, filter, 2x sponges. The blot chamber was placed in an electrophoresis chamber and filled inside with blot buffer and on the outside with deionized water. Blotting took place at 30 V and 300 mA for 90 min. The membrane was then removed and blocked with 5 % milk powder TBS in a 50 mL Falcon tube at room temperature for 20 min on the roller mixer. The SDS gel was then stained with InstantBlue as described above, to check the blotting success. After blocking, the membrane was incubated with a primary antibody. For this, the PVDF membrane was incubated overnight on the roller mixer at 4 °C in a 50 mL Falcon tube containing 5 mL TBS (5 % milk powder), 125 μL 20 % Tween20 and 1:1000 diluted antibody. After incubation with the primary antibody, the membrane was washed three times for 5 min in wash buffer (TBS 0.05 % Tween20) before loading with the secondary antibody. The membrane was then incubated with the horseradish peroxidase (HRP) conjugated secondary Ab diluted 1:10000 in blocking buffer for 1 hour at room temperature. The method of indirect staining with a secondary antibody was used to amplify the signal (see Fig. 9. After incubation, the membrane was washed

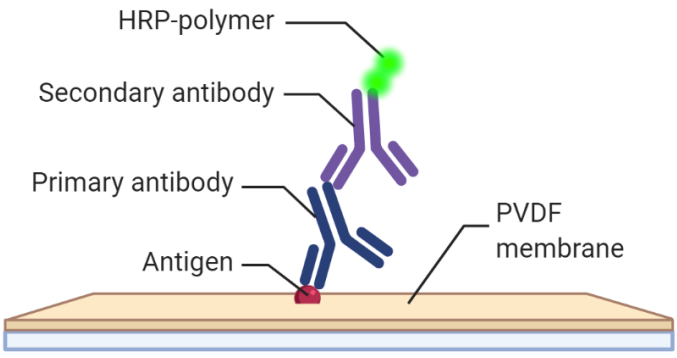

Figure 9 Immunolabeling. The PVDF membrane was incubated with the antigen specific primary antibody and washed before the secondary antibody was added. This secondary antibody was conjugated with horseradish peroxidase (HRP) which can be detected on film with a developer. It recognizes all types of antibodies from a specific host species, e.g., rat or mouse. This indirect staining is more sensitive than direct staining with only single (primary) antibody conjugated with HRP due to signal amplification. Another advantage is, that secondary antibodies can be used against many different primary antibodies from the same species the same time to detect different antigens. Adapted from "Immunohistochemistry on tissue layer", by BioRender.com (2021) [48].

three times with wash buffer. The developer cassette was exposed to light for at least one minute. After equilibration using ECL kit, the membrane was wrapped in cling film and fixed in the cassette with adhesive tape. In darkness or red light, a film was placed on the membrane for a specified exposure time with the frame closed and de-

veloped with the developer machine. The position of the membrane, as well as the markers, were marked with a pen on the film and the exposure time was noted before it was scanned for further evaluation.

4.2.4 Production of single-wavelength ATP sensors in bacteria

For protein production 50 μL of transformants carrying the respective construct were streaked on 2xYT kan agar and incubated overnight at 37 °C. One single colony was picked and used to inoculate 10 mL of 2xYT kan medium. The cultures were incubated at 37 °C in a shaker at 180 rpm overnight. Overnight cultures were centrifuged at 4600 rpm for 10 min and the supernatant was discarded. The pellet was resuspended in 10 mL 2xYT kan medium. For the main culture, 200 mL 2xYT kan medium were inoculated with 4 mL cell suspension (1:50) in an Erlenmeyer flask. The culture was incubated for two to four hours at 37 °C in a shaker at 220 rpm. A photometer was used to determine the optical density at 600 nm. When $OD_{600\,nm}$ reached a value between 0.3 and 0.6, 1 mM IPTG was added. After further incubation for 3 h at 30 °C shaking, the culture was transferred to 200 mL Sorvall centrifuge tubes and centrifuged at 4600 rpm and 4 °C for 15 min. The supernatant was discarded, and the cell pellet was stored at -80 °C until use.
Cell pellets were removed from the -80 °C freezer and the weight of the pellet was determined. 1 g of wet pellet was lysed in 5 mL of lysis buffer incubated for 30 min at room temperature (RT) rolling. The suspension was transferred to Sorvall centrifuge tubes and centrifuged for 60 min at 20000 rpm and 4 °C. The supernatant (total cell lysate) was transferred to 50 mL Falcon tubes and the pellet containing cell debris was discarded.

4.2.5 Protein purification with affinity chromatography

Ni-TED Both His-tagged TP1170_HHM1.1 sensors were purified with nickel-tris-carboxymethyl ethylene diamine (Ni-TED) affinity chromatography resin using Protino Ni-TED gravity flow column. The column was equilibrated with 320 μL of LEW buffer before loading the cell lysate. After washing twice with 320 μL of LEW buffer, the sensor was eluted by rinsing the column three times with 240 μL of 1x elution buffer. To evaluate the purification success, the following fractions were collected: loaded sample (diluted 1:5), flowthrough, the two wash fractions and the three elution fractions (diluted 1:2). Samples were applied to SDS-PAGE using a 10 % Bis Tris gel (see 4.2.2).

Talon ATPOS was purified at CSSB using a Talon fast protein liquid chromatography (FPLC) column. ÄKTA™pure was used as chromatography system. The ÄKTA was prepared first. Waste-outlet 1 was equipped with 100 mL Schott bottle and fraction collector with 2x 50 mL Falcon tubes was placed on position 1, and a 96 deepwellblock

on position 2. A new manual run was started. Tubes A1, B1 and sample pump S1 were flushed with ddH_2O. Afterwards, B1 was flushed with elution buffer and 1 mL Talon column was connected via drop-to-drop to column bypass 1 with a flowrate of 0,5 mL/min ddH_2O from tube A1. Then the column was washed with 5 CV (column volume) ddH_2O. Tube A1 was transferred to loading buffer (1x PBS) and the column was equilibrated with at least 5 CV or until conductivity was stable. In the next step, S1 was transferred to loading buffer and flushed again. Furthermore, waste outlet 1 and fraction collector were washed with loading buffer. The bacterial lysate was applied to the loading device, S1 was placed inside and loading was initiated with 1 mL/min via injection valve direct load. Flowthrough was collected in a Schott bottle connected to waste-outlet 1 and 20 μL were taken for SDS-PAGE. After successful loading, the valve was switched from S1 to A1 and the column was washed until a stable UV280 baseline. This washing step was collected in 30 mL fractions in 50 mL Falcon tubes and 20 μL were taken for SDS-PAGE. After reaching the UV280 baseline, linear imidazole gradient was initiated from 0 % B1 to 100 % B1 over 15 CV (0 mM imidazole - 250 mM Imidazole). Fractions of 2 mL were collected in 96-deepwell block. The mAU was observed for increasing values and if it increased drastically, the proportion of B1 was kept constant until the peak came back to baseline. After that, settings were changed to the gradient. When 100 % B1 was reached, the column was washed first with 5 CV ddH_2O and afterwards with the same amount of 20 % EtOH for storage. The column was disconnected drop-by-drop in 20 % EtOH. In the end A1 and S1 were also flushed first with ddH_2O and then with 20 % EtOH (system wash).

StrepTactin The sensors TP1170_HHM1.1 and TP1170_HHM1.1_RRKK were purified in a second step using a Strep-Tactin©XT 4Flow© gravitiy flow column. The column was prepared by filling 2 mL of StrepTactin matrix into in a 15 mL column between two frits. The matrix was then washed with 2x 2 CV of PBS -/-. The bacterial lysate was then added onto the column and washed three times with 2 mL wash buffer (buffer W). Then in six additional steps, 0.5 mL elution buffer (buffer BXT) was added, and 0.5 mL samples were collected. To confirm the purification success, SDS-PAGE (see 4.2.2) was performed with loaded samples from every fraction.

4.2.6 Determination of protein concentration using BCA assay

The BCA kit from Thermo Scientific was used for the determination of protein concentration. In a 96-well-plate a dilution series (range 0.016 - 2 mg/mL) of a BSA standard and blanks were applied. Standards and samples were prepared as duplicates. To make sure the unknown sample is in the range of the standard, a serial dilution of the sample was prepared. The respective medium of the samples or deionized water was used for dilution. In each well, 10 μL sample and 200 μL reaction mixture (50 parts reagent A

and 1 part reagent B) were mixed und the plate incubated at 37 °C for 30 min. After incubation, absorbance was measured at 562 nm with the Perkin Elmer multilabel counter. To determine the protein concentration of the unknown sample, standard curve was calculated from the OD_{562nm} of the BSA dilutions. By determining the slope (m) and intercept (b), the unkown concentration is calculated with the dilution factor and the following linear equation:

$$A = m \cdot c + b$$

with A = absorbance and c = concentration.

4.2.7 Protease digest

To remove the 14xHis tag after affinity chromatography (Ni-TED or Talon column) and buffer exchange, NEDP1 protease was used. NEDP1 cleaves the protein, recognizing a unique, short recognition motif the NEDD8 domain (see 9). The protease was provided by Philipp Schmidt of AG Haag. Protease was used diluted 1:20 (c = 1.94 μg/mL) with the sample and incubated on roller mixer at 4 °C for three days or at room temperature overnight.

4.2.8 Labeling of proteins via maleimide chemistry

The purified ATPOS was labeled with Cy3-maleimide via maleimide coupling. For this purpose, the purified protein (after protease digest and second purification with Talon resin) was incubated with 100-fold molar excess of TCEP for 20 min at room temperature on roller mixer to reduce disulfide bonds. 1 mg Cy3-maleimide was dissolved in 100 μL DMSO. 20-fold excess of the dye was added to the reduced protein solution and incubated overnight at room temperature. The mixture was then concentrated using an Amicon column with a cutoff of 3000 kDa at 4 °C and 4600 rpm. Size exclusion chromatographyand to separate unbound Cy3-maleimide was performed by the staff of CSSB.

4.2.9 ATP detection

To evaluate ATP sensor function, each sensor was used undiluted with different concentrations of ATP in 96-well-plate diluted in PBS. Fluorescence intensity at 535 nm was detected using the multilable counter. Fluorescence of ATPOS was also measured with a plate reader over a period of time before and after adding ATP.

4.3 Methods in cell biology

4.3.1 Thawing cells (PBMCs)

All steps were performed under a class 2 safety cabinet to provide sterile conditions. The cells were stored at -80 °C and thawed in a 37 °C water bath. The cells were added immediately to 9 mL of prewarmed RPMI complete medium. In the next step, the cell suspension was centrifuged at 1300 rpm at 4 °C for 5 min. Supernatant was discarded and the pellet was dissolved in RPMI complete medium. After being washed twice with medium, the cell number was determined using the Neubauer counting chamber (see 4.3.3) and the cells were adjusted to the desired cell concentration.

4.3.2 Culture and passage of suspension cells

The suspension cells were cultivated in RPMI complete medium in 10 cm Petri dishes at 37 °C and 5 % CO_2. Cells were split twice a week and diluted 1:5 or 1:10 (depending on cell growth) with fresh medium in a fresh Petri dish.

4.3.3 Cell counting

For cell counting, the cell pellet was resuspended in a defined volume of medium. 10 μL of the cell suspension was diluted 1:10 with trypan blue. The latter was used to stain dead cells. 10 μL of the mixture was pipetted between the counting chamber and the coverslip of the Neubauer chamber. The cell number was determined under the light microscope at 40x magnification. Live cells were counted in two of the four large outer squares (16 individual squares each) and the mean of the two cell counts was calculated.
Calculation of cell concentration:
Cells/mL = counted cells x 10^4 (chamber factor) x dilution factor.

4.3.4 Cell preparation for flow cytometry

To detect cell surface expression of proteins, flow cytometry was used. Cells were resuspended in PBS and centrifuged at 1300 rpm for 5 min at 4 °C. The supernatant was discarded, and the cell pellet was dissolved in the remaining liquid using a vortexer. Fluorochrome conjugated antibodies were then added and incubated for 30 min on ice in the dark. The stained cells were mixed with 2 mL of PBS and centrifuged again at 1300 rpm for 5 min at 4 °C. The supernatant was discarded and the sample was fixed with 1 % PFA unless measured within 6 h (4.2.1).

4.3.5 Binding experiments

The binding of sensors to beads and cells were evaluated with different methods to bring the ATP sensors close to the cell surface. This strategy was necessary to be

able to measure local concetration of extracellular ATP in close proximity to the cell membrane.

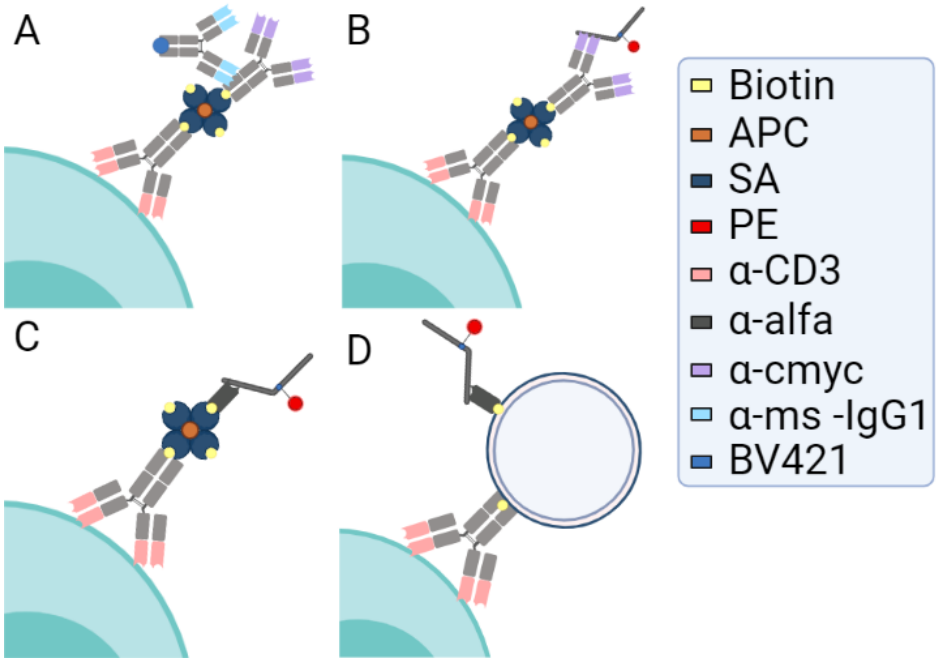

Figure 10 ATPOS binding to beads or streptavidin. (A) Biotinylated CD3 Ab binds to the cell surface and to APC-conjugated streptavidin (SA). The SA is also labeled with biotinylated cmyc-antibody from mouse as host species. SA-cmyc binding is monitored with anti-ms-IgG1-antibody conjugated with BV421. (B) The ATPOS sensor is loaded onto the SA-antibody complex via its cmyc tag recognized by cmyc antibody. (C) The ALFA tag recognizing nanobody (ALFA Nb) is used instead of cmyc antibody to bind ATPOS to the SA. (D) Instead of soluble SA, SA-coated transparent 5 μm beads are used to bring ATPOS to cell surface. Created with BioRender.com.

Bio-layer Interferometry Biomolecular interactions were measured via bio-layer interferometry (BLI) using the BLItz Instrument (ForteBio/Sartorius). The single-use High Precision Streptavidin (SAX) and Protein A Biosensors (Dip and ReadTM, FortéBio) were used to evaluate antibody binding. In the first step, initial baseline was measured for 20 s to detect background signal intensity. Then the antibody was loaded to the sensor for 45 s and a following second baseline was measured for 45 s to exclude dissociation of loaded antibody. In the next step, association of the protein of interest occurred for 120 s until the equilibrium was reached followed by dissociation (in buffer) for additional 120 s. The observed wavelength shift, reflects the change in thickness of the bio-layer due to the binding or detachment of molecules (see Fig. 11). ATPOS binding was tested with either biotinylated cmyc-antibody (clone 9E10) and biotinylated ALFA-nanobody immobilized on SAX or ALFA-nanobody-rabbit IgG immobilized on Protein A biosensors. TP1170_HHM1.1 and TP1170_HHM1.1_RRKK interactions were measured with biotinylated cmyc-antibody bound to SAX biosensor.

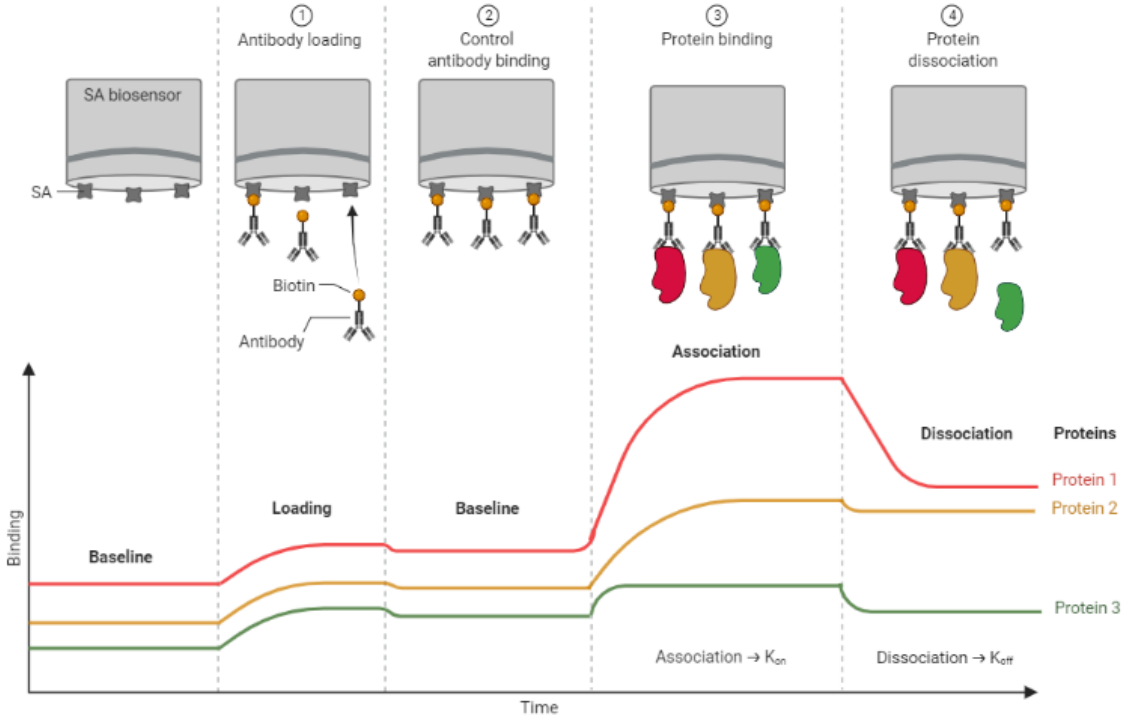

Figure 11 Bio-layer Interferometry principle. The initial baseline is detected with the biosensor in kinetics buffer (phosphate buffered saline (PBS) 0.01 % BSA, 0.002 % Tween20). (1) The biotinylated antibody or nanobody is loaded on the SA coated biosensor and (2) it is washed with kinetics buffer to control binding. (3) Protein sample is loaded, and association takes place. (4) The biosensor is washed with kinetics buffer again to monitor dissociation. Protein 1 was not diluted in kinetics buffer first, so its own buffer components effected the binding or the biosensor. Protein 2 is a larger protein than protein 1 and protein 3 and it binds strongly. Protein 3 is a smaller protein. It binds weakly and falls off when washed with buffer. Adapted from "Biolayer Interferometry", by BioRender.com (2021) [48].

Beads To confirm the function of ATPOS, several experiments with transparent SA coated beads were performed (see Fig. 10 D). Therefore, the beads (0.5 μl beads per tube) were added to 1 mL PBS and centrifuged at 13,000 rpm for 3 min to wash them. Biotinylated anti-CD3 Ab and biotinylated anti-ALFA Nb were mixed and the beads were added. After 20 min of incubation, the beads were washed again and mixed with ATPOS. The beads were incubated for 20 min and washed afterwards. For FACS measurements all steps were performed in FACS tubes with different Ab-Nb-ratios in each tube. For analysis with confocal microscopy the beads were transferred to an 8-well μ-Slide and ATP was added (60 - 500 μM).

Streptavidin-linked cell coupling To bring the sensor close to the cell surface, soluble SA was used as a linker (see Fig. 10 A - C). In the first experiments, staining was performed stepwise. Jurkat cells or PBMCs were used in FACS measurements. The cells were washed and labeled first with b-CD3 Ab. After every step of staining the cell suspension was incubated for 30 min and washed twice with PBS at 13,000 rpm for

5 min. Fluorochrome labeled SA was used as a checkpoint to confirm that the complex shown in Figure 10 was bound to the cell. In the first trials with ATPOS, b-cmyc was used to bind the sensor to SA. As an alternative, the nanobody against the ALFA tag was biotinylated and used instead.
In following experiments, the premixed b-CD3 Ab and b-ALFA Nb were mixed with SA and added to the cells. For FACS measurements, all the steps were performed in FACS tubes with different Ab-Nb-ratios in each tube. For analysis with the microscope, the cells were transferred to an 8-well μ-Slide and ATP was added (60 - 500 μM). To immobilize Jurkat cells to the slide, each well was incubated with 150 μL poly-L-lysine for 25 min and left to dry before 100 μL cells were added. After 1 h of incubation, 150 μL RPMI complete medium were added onto the cells and the slide was incubated overnight at 37 °C and 5 % CO_2. Prepared SA-ATPOS or beads-ATPOS complexes were added and incubated for 30 min before measuring.

5 Results

This thesis was aimed to construct fluorescent sensor molecules for the detection of local concentrations of extracellular ATP. The two sensors, TP1170_HHM1.1 and ATPOS, and their RRKK variants were constructed based on the work of Lobas *et al.* (2019) and Kitajima *et al.* (2020). Sequences coding for those sensors were cloned into bacterial vector plasmids (see section 3.9) and the protein expressed in *Escherischia coli*. Both sensors were purified and the His tag cleaved from the sensor molecules before testing (see Fig. 12). Additionally, ATPOS was labelled with Cy3-maleimide prior to binding tests. As a control, two point mutations (arginine to lysine) were introduced into the binding domain to gain a nonfunctional sensor named TP1170_HHM1.1_RRKK and ATPOS_RRKK, respectively. In the following molecule production and binding test results are described first for TP1170_HHM1.1 and in the second section for ATPOS.

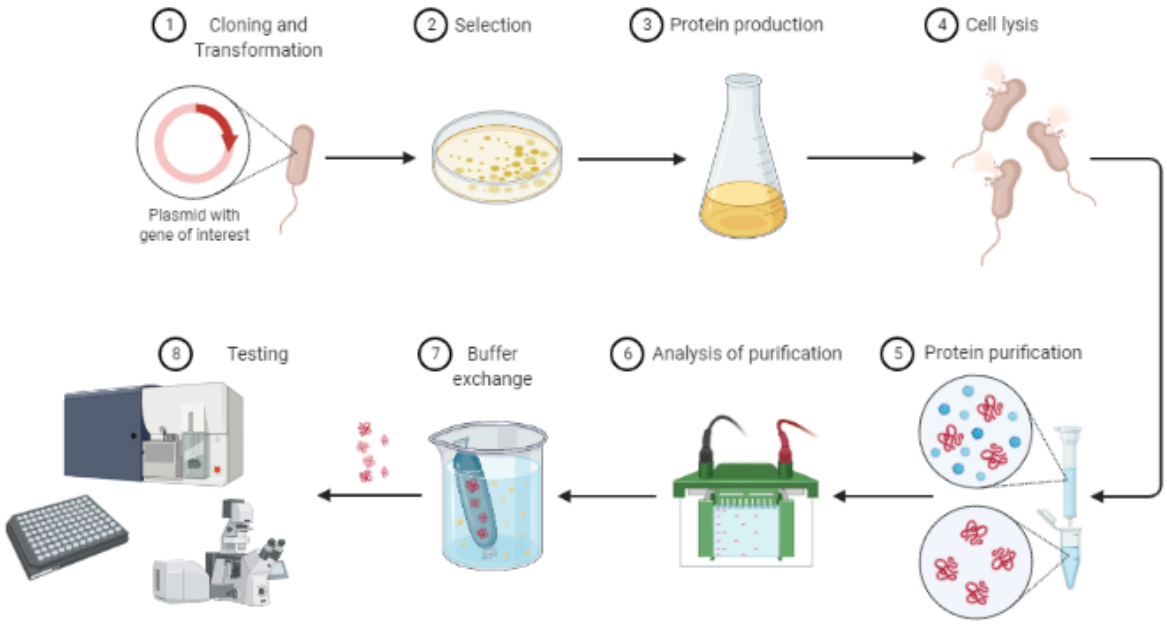

Figure 12 Workflow for TP1170_HHM1.1 and ATPOS ATP sensor cloning, bacterial expression, purification and ATP binding experiments. (1) The gene of interest was inserted into a bacterial vector plasmid and introduced into competent *E. coli* BL21 cells. (2) The transformed bacteria were streaked, and single colonies were picked for preculture. (3) Main culture was inoculated and incubated for several hours before starting protein expression by adding IPTG. The cells were harvested and (4) lysed by lysis buffer. (5) The target protein was purified using affinity chromatography and modified. The 14xHis tag was cleaved by NEDP1 protease. (6) The purification success was analyzed via SDS-PAGE and Western blot. (7) Buffer was changed to 1x PBS and concentration was increased using an Amicon column. (8) The purified sensor was tested in experiments in solution (96-well-plates) or coupled to beads or cells (FACS, microscope). Adapted from "Protein Overexpression and Purification from Bacteria", by BioRender.com (2021) [48].

5.1 Single wavelength sensor TP1170_HHM1.1

5.1.1 Cloning, production and purification

TP1170_HHM1.1, used in this thesis, is based on the HHM1.1 ATP sensor developed by Lobas *et al.* (2019). Lobas *et al.* cloned a modified version of GFP (cpSFGFP) inside the ATP binding domain. ATP binding induced conformational change leads to an increased fluorescence of the GFP.

The sensor's sequence and its RRKK variant were ordered from Addgene. Each gene block was then cloned into a bacterial vector plasmid (gene map in 9. Appendix). The vector contained the sequence coding for TP1170 nanobody combined with 14xHis and TwinStrep tag as well as kanamycin resistance. The nanobody was chosen due to its ability to recognize and bind mouse κ-chain Abs. The vector plasmid was prepared by Philipp Schmidt of AG Haag.

The fusion protein was produced in *E. coli* and purified by affinity chromatography using a StrepTactin or a Ni-TED column. The 14xHis tag was cleaved by NEDP1 protease and a second chromatography was performed using Ni-TED column. SDS-PAGE and Western blot analysis were performed to confirm the expression and to monitor purity of the target protein after each purification step (see Fig. 13). The cell

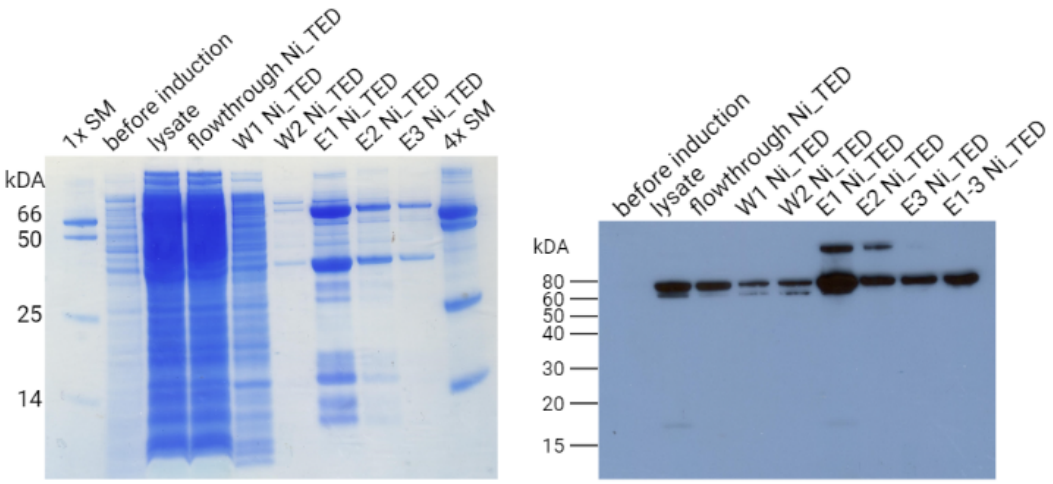

Figure 13 SDS-PAGE and Western blot analysis of TP1170_HHM1.1 expression and purification. Purification with Ni-TED column was analyzed using SDS-PAGE (left) and Western blot (right). In SDS-PAGE 10 μl of each fraction were loaded undiluted. For Western blot analysis some samples were diluted 1:5 (lysate, flowthrough, W1) or 1:2 (E1, E2, E1-3). SDS-PAGE was performed at 200 V for 40 min and the gel was stained overnight with InstantBlue. Western blot samples were blotted on PVDF membrane and blocked with 5 % milk powder solution. Signals were detected using StrepTactin conjugated with HRP (diluted 1:1000 in 5 % milk powder solution). Bands of TP1170_HHM1.1 sensor were detected around 75 kDa.

lysate and all chromatography fractions containing the target protein showed a light greenish color because of the GFP. The total protein yield of TP1170_HHM1.1 (ca.

0.41 mg) was much higher than the yield of TP1170_HHM1.1_RRKK (ca. 39 μg). Both proteins still showed contamination in SDS-PAGE after purification. Results of SDS-PAGE and western blot analysis after purification with Ni-TED clumn are shown in Figure 13 . As shown in the left part of the figure, several other bands were visible in SDS-PAGE besides the one of the target protein at 75 kDA. The sensor molecule was detected in all fractions except the sample, which was taken before induction. It was expected to be present in lysate and in the elution fractions.

5.1.2 Binding tests

The TP1170 nanobody was chosen as a fusion partner to bring the ATP sensor HHM1.1 in contact with the cell surface to detect local ATP concentrations. The nanobody was designed by Pleiner *et al.* (2018) to recognize and bind the κ light chain of mouse antibodies. Due to its basic green fluorescence, the sensor could be detected even in

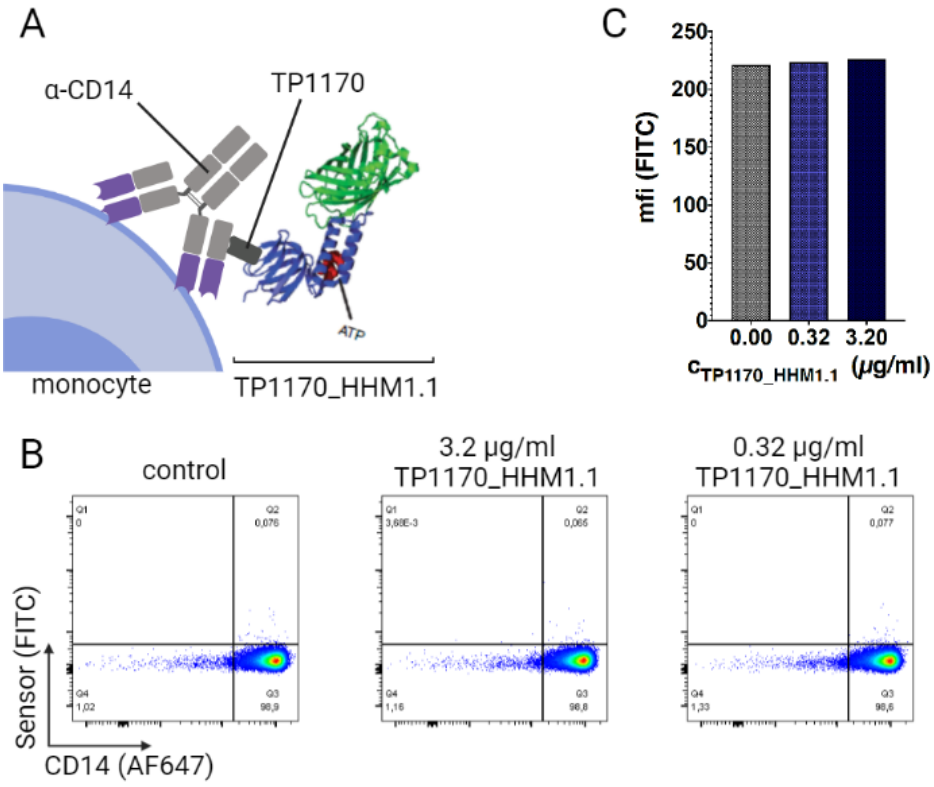

Figure 14 TP1170_HHM1.1 binding to monocytes. (A) Schematic overview of TP1170_HHM1.1 binding to anti-CD14 mouse Ab. The TP1170 nanobody recognizes the κ light chain of the mouse Ab which is bound to its antigen, expressed on the cell surface. (B) Monocytes were gated and sensor (FITC) was plotted against anti-CD14 (Alexa Fluor 647). (C) Median fluorescence intensity (mfi) is plotted against sensor concentration. There is no significant difference between control (grey), 0.32 μg/mL (blue) and 3.2 μg/mL (black) TP1170_HHM1.1. (A) Created with BioRender.com.

absence of ATP in the FITC channel of FACS or at 535 nm with the multilabel counter. Binding to antibody coated soluble streptavidin, SA-beads or cells directly were tested

and analyzed with flow cytometry.

To recruit the sensor to the cell surface, monocytes (provided by Samantha Eiberg) were coated with Alexa Fluor 647 conjugated anti-CD14 mouse antibody and incubated with two different concentrations of TP1170_HHM1.1 (3.2 μg/mL and 0.32 μg/mL) (see Fig. 14). Figure 14 C shows the gating strategy; monocytes were gated first. Then sensor (FITC channel) and CD14 were plotted against each other. As shown in Figure 14 B the median fluorescence intensity (mfi) of the monocytes did not increase significantly with higher concentration of TP1170_HHM1.1, suggesting that only a few sensor molecules bound to antibodies on cell surface.

In a second experiment, TP1170_HHM1.1 was supposed to bind to SA coated transparent 5 μm beads coated with a biotinylated anti-CD3 mouse antibody (see Fig. 15 A). As a negative control, beads were coated with biotinylated anti-CD25 rat antibody.

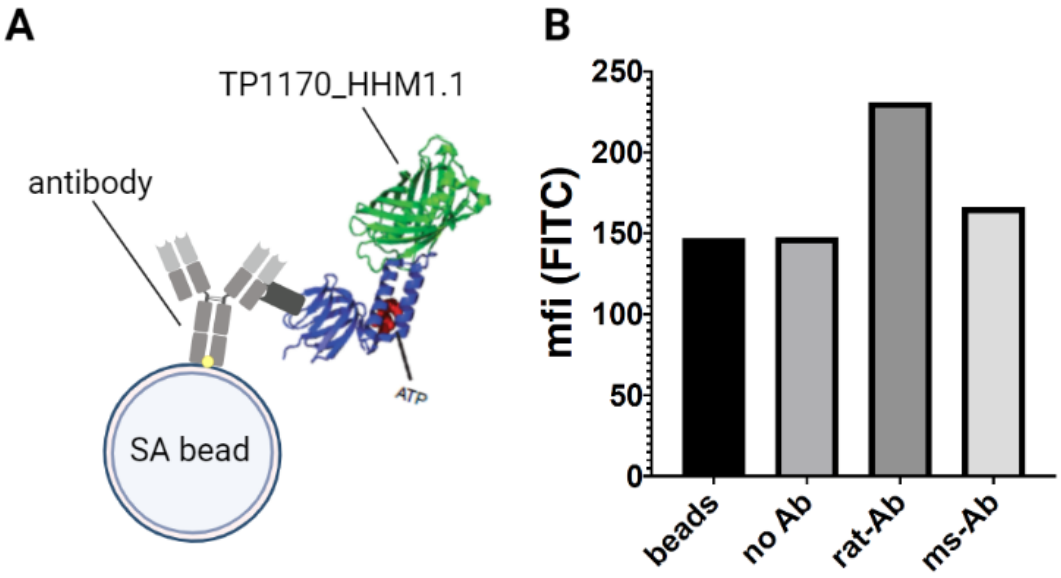

Figure 15 Test specific binding of TP1170_HHM1.1. to mouse antibodies. (A) Binding of TP1170_HHM1.1 is shown schematically. SA coated beads are labeled with biotinylated antibodies. B-CD3 mouse Abs and b-CD25 rat Abs are used to test specfic binding of the nanobody to mouse κ light chain. (B) The results show higher mfi in presence of rat Ab than binding to mouse Ab, suggesting that TP1170 Nb bound unspecifically. (A) was created with BioRender.com.

The nanobody should only bind to the κ light chain of b-CD3. Analysis with flow cytometry showed, with mfi of 231, higher fluorescence in presence of rat antibody than when the sensor was incubated with mouse antibody (mfi = 166) (see Fig. 15 B). Figure 15 B shows there was also a high background signal with mfi at 147. Mfi did not increase significantly in presence of mouse antibody (Δmfi = 19). It stayed almost at the same level as without any antibody present. Almost no fluorescence was detected in the negative control (only beads) with mfi of 147 and in absence of antibodies but after incubation with sensor with mfi of 147.5, suggesting that only a few sensor molecules bound to mouse Abs.

Another approach was to couple the sensor to the SA-beads via its TwinStrep tag. Analysis with flow cytometry showed no significant increase in fluorescence after ATP application (see Fig. 16). Without sensor added, mfi was at 148 and at 173 with 3.2 μg/mL TP1170_HHM1.1, the highest concentration used in this experiment. The mfi for 0.32 μg/mL and 1.1 μg/mL sensor was almost the same with a mfi of 164.5 and 163.5.

Before the next tests were done, a new batch TP1170_HHM1.1 was produced and

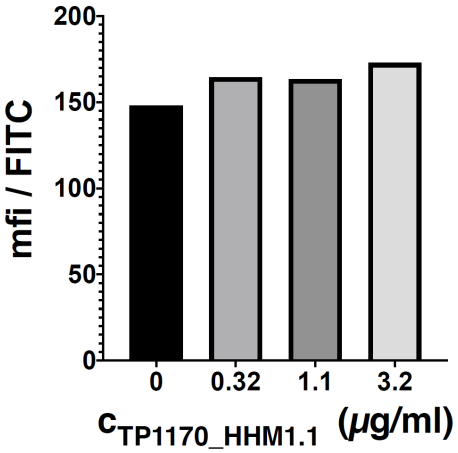

Figure 16 Binding TP1170_HHM1.1 to SA coated beads via its TwinStrep tag. SA coated transparent 5 μm beads were incubated with different concentrations of TP1170_HHM1.1 (0; 0.32; 1.1 and 3.2 μg/mL) and analyzed with flow cytometry. mfi (FITC) of the beads was plotted against sensor concentration. No significant increase of mfi could be observed.

TP1170_HHM1.1_RRKK was cloned, expressed and purified. Both sensor constructs were tested with Jurkat cells and with SA coated transparent beads (see Fig. 17 A - C). Different volumes (0 - 5 μL) of sensor stock solution were added. The concentration of the RRKK's stock solution was lower by a factor of 10 compared to TP1170_HHM1.1. Without any sensor (0 μL) beads showed mfi of 33.7. When 0.5 μL of TP1170_HHM1.1 stock solution ($c_{TP1170\_HHM1.1} = 0.32$ mg/mL) was added, mfi showed an increase to 146. With 1 μL added, there was a mfi of 186. Due to its lower concentration, only the two highest volumes (2 μL and 5 μL) were added in comparison of the two sensor variants. Mfi was higher for TP1170_HHM1.1 with values of 457 (2 μL) and 842 (5 μL) than for TP1170_HHM1.1_RRKK with 256 (2 μL) and 392 (5 μL). TP1170_HHM1.1 almost doubled its mfi from 2 μL to 5 μL while TP1170_HHM1.1_RRKK showed an increase of approximately 50 %. In the cell experiments, the values were closer together. Without any sensor (0 μL) beads showed mfi of 105. When 0.5 μL of TP1170_HHM1.1 stock solution was added, mfi showed an increase to 126. With 1 μL added, there was a mfi of 152. Like in the bead experiment, 2 μL and 5 μL of TP1170_HHM1.1_RRKK were added in comparison with TP1170_HHM1.1. Mfi was higher for TP1170_HHM1.1 with values of 235 (2 μL) and 266 (5 μL) than for TP1170_HHM1.1_RRKK with 168

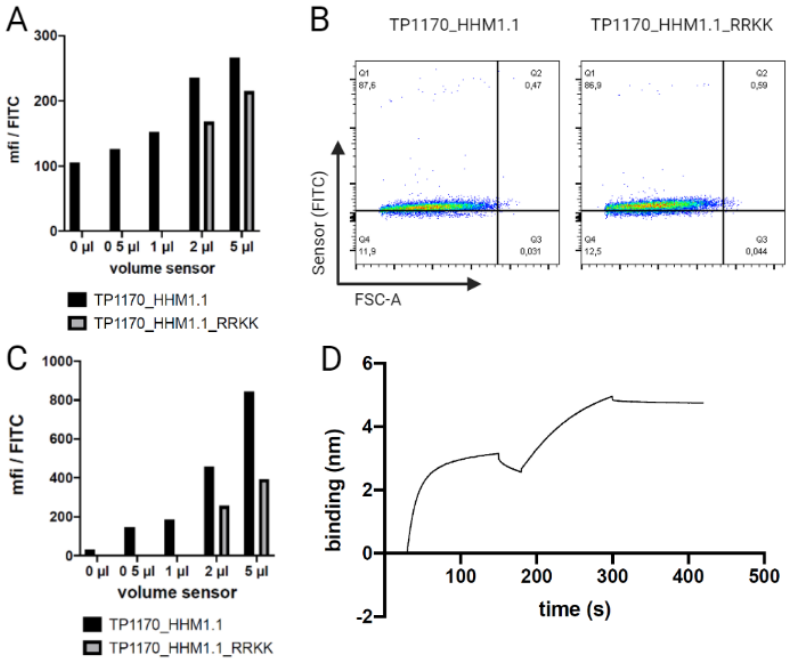

Figure 17 Binding of TP1170_HHM1.1 and TP1170_HHM1.1_RRKK to Beads and Jurkat cells. (A) Jurkat cells were coated with fluorochrome conjugated anti-CD3 Ab. Sensor was added (stock solutions: $c_{TP1170\_HHM1.1} = 0.32\,mg/mL$ and $c_{TP1170\_HHM1.1\_RRKK} = 0.03\,mg/mL$). The stained cells were analyzed with flow cytometry. The mfi of the gated Jurkat cells was plotted against the used sensor volume. With higher sensor concentration, fluorescence increased. (B) SA coated beads were labeled with b-CD3 Ab and incubated with TP1170_HHM1.1 (stock solutions: $c_{TP1170\_HHM1.1} = 0.32\,mg/mL$) or TP1170_HHM1.1_RRKK (stock solutions: $c_{TP1170\_HHM1.1\_RRKK} = 0.03\,mg/mL$). In analysis with flow cytometry, mfi of the beads was detected and the measured events in FITC channel (sensor) were plotted against forward scatter (FSC). (C) The mfi increased with higher concentrations of each sensor. TP1170_HHM1.1 and TP1170_HHM1.1_RRKK showed same behavior but higher signals in presence of TP1170_HHM1.1. (D) The binding of TP1170_HHM1.1 to mouse κ light chain Abs was analyzed with BLItz. Biotinylated cmyc Ab was loaded onto Protein A biosensor and association of the ATP sensor was observed after measuring the second baseline. No significant dissociation was detected, suggesting a strong binding.

(2 μL) and 215 (5 μL). Both showed no significant increase of fluorescence. Binding of TP1170_HHM1.1 to a mouse κ-chain antibody (b-cmyc) was confirmed by BLItz measurements (see Fig. 17 D).

5.1.3 ATP sensor function

The responsiveness of the TP1170_HHM1.1 sensor to ATP was tested first in solution and in direct comparison to its negative control TP1170_HHM1.1_RRKK. For this purpose, a black 96-well-plate was used for measurements at the multilabel counter. As described in Figure 18, TP1170_HHM1.1 showed the highest signal without ATP added around a mfi of $1.30 \cdot 10^7$. Fluorescence decreased to $1.22 \cdot 10^7$ in presence of 1 μM ATP and further to $1.20 \cdot 10^7$ with 10 μM ATP added. The lowest signal was reached

at $1.11 \cdot 10^7$ with 25 μM ATP present. When 50 μM ATP were added, signal was almost as high as without ATP with a value of $1.25 \cdot 10^7$. TP1170_HHM1.1_RRKK showed similar behaviour. The highest signal was $1.49 \cdot 10^7$ in presence of 1 μM ATP. Without ATP, fluorescence was at $1.26 \cdot 10^7$. Detected fluorescence signal decreased in presence of 10 μM ($1.08 \cdot 10^7$) and 25 μM ATP ($8.78 \cdot 10^6$) and showed an increase to $1.23 \cdot 10^7$ with 50 μM ATP present. As control, PBS was measured in absence of ATP with a signal around $2.36 \cdot 10^5$ and with 50 μM ATP around $2.53 \cdot 10^5$. Since the two sensor variants showed so similar behavior and no significant responsiveness to ATP, no further experiments were performed.

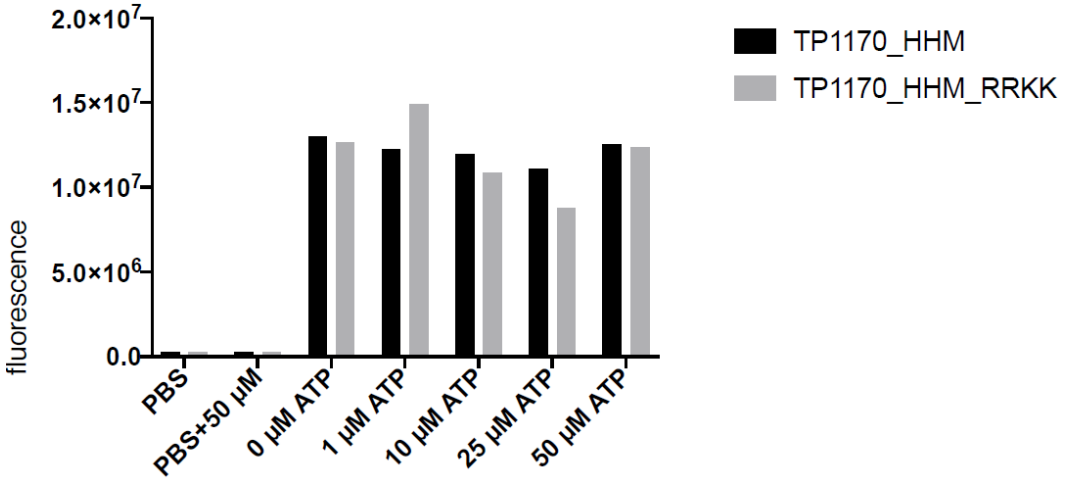

Figure 18 Evaluation responsiveness of TP1170_HHM1.1 and TP1170_HHM1.1_RRKK to ATP. The two sensor constructs TP1170_HHM1.1 ($c_{TP1170\_HHM1.1} = 0.32$ mg/mL) and TP1170_HHM1.1_RRKK ($c_{TP1170\_HHM1.1\_RRKK} = 0.03$ mg/mL) were incubated with different ATP concentrations (1 - 50 μM) for 2 min in PBS and fluorescence was detected at 535 nm at the multilabel counter. As control PBS with and without ATP was measured. Both constructs showed similar behavior despite RRKK's concentration was lower than that of TP1170_HHM1.1 by a factor of 10.

5.2 Small molecule sensor ATPOS

5.2.1 Cloning, production and purification

ATPOS was constructed according to Kitajima *et al.* (2020). They labeled the ATP binding domain (ϵ-subunit of the F0F1-ATPase from *Bacillus* PS3) with a fluorescent dye. Conformational change due to ATP binding leads to an increase in fluorescence, which can be detected.

Gene block coding for this ATP binding domain fused to cmyc/ALFA tag and its RRKK variant were obtained from Addgene and cloned into the same bacterial vector as TP1170_HHM1.1. The protein contained a 14xHis tag besides the cmyc and the ALFA tag (gene map in appendix). In cooperation with the Protein Production Core Facility (PPCF) at the Centre for Structural Systems Biology (CSSB), the sensor was

produced and purified according to the procedure of Kitajima *et al.*
The protein was expressed in *E. coli* and purified by affinity chromatography using a 1 ml FPLC Talon column and ÄKTA system with linear imidazole gradient. To identify the fractions for subsequental purification, SDS-PAGE was performed (see Fig. 19). Those fractions were pooled and buffer was exchanged to PBS via dialysis. After protease digest overnight, the sample was purified with the Talon column again to separate the cleaved His tag and all uncleaved protein. Cleavage of the His tag was confirmed via SDS-PAGE afterwards. The purified protein was labeled with Cy3-maleimide and unbound dye was separated using size exclusion chromatography. According to the chromatogram, the ATPOS sensor eluted earlier than expected (data not shown). SDS-PAGE confirmed that the fraction of the peak in question contained the target protein. Presumably, dimers had formed during the purification and modification process. Protein yield of purified protein was about 350 μg.

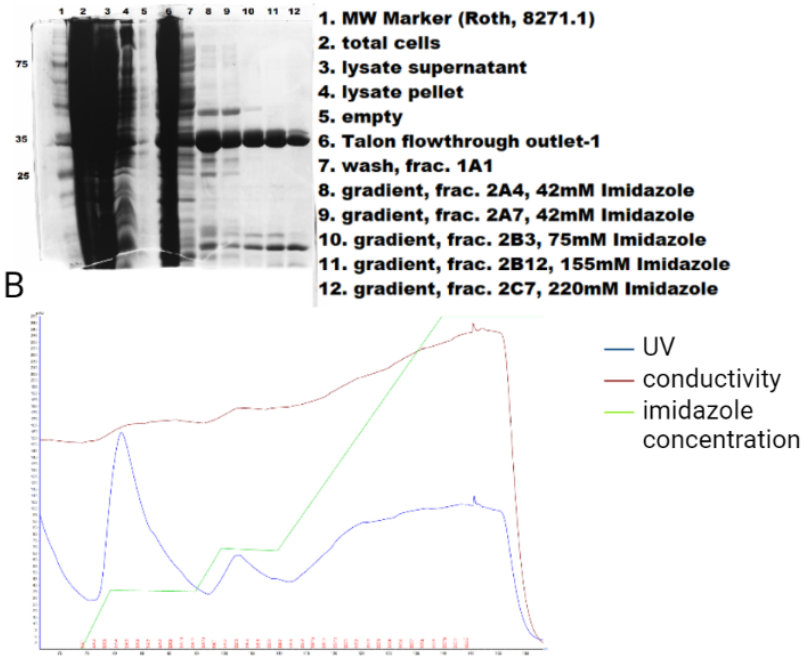

Figure 19 SDS-PAGE analysis of ATPOS purification via Talon column. First purification step using Talon column was analyzed using SDS-PAGE. (A) 10 μl of each fraction were loaded undiluted onto a 12 % gel. SDS-PAGE was performed at 180 V for 70 min and stained overnight with InstantBlue. Bands of the ATPOS sensor were detected around 32 kDa. The chromatogram (B) of the purification showed which fractions should be analyzed with SDS-PAGE. UV-peaks were an indicator for protein elution in general.

5.2.2 Binding tests

To bring the ATPOS molecule close to the cell surface, cmyc tag was used to bind the sensor to beads or soluble SA. Therefore, a complex of ATPOS, b-cmyc antibody, SA-coated beads or soluble SA and a biotinylated antibody against an antigen expressed on cell surface were formed (see 4.3.5). Due to the labeled Cy3, the ATPOS could be

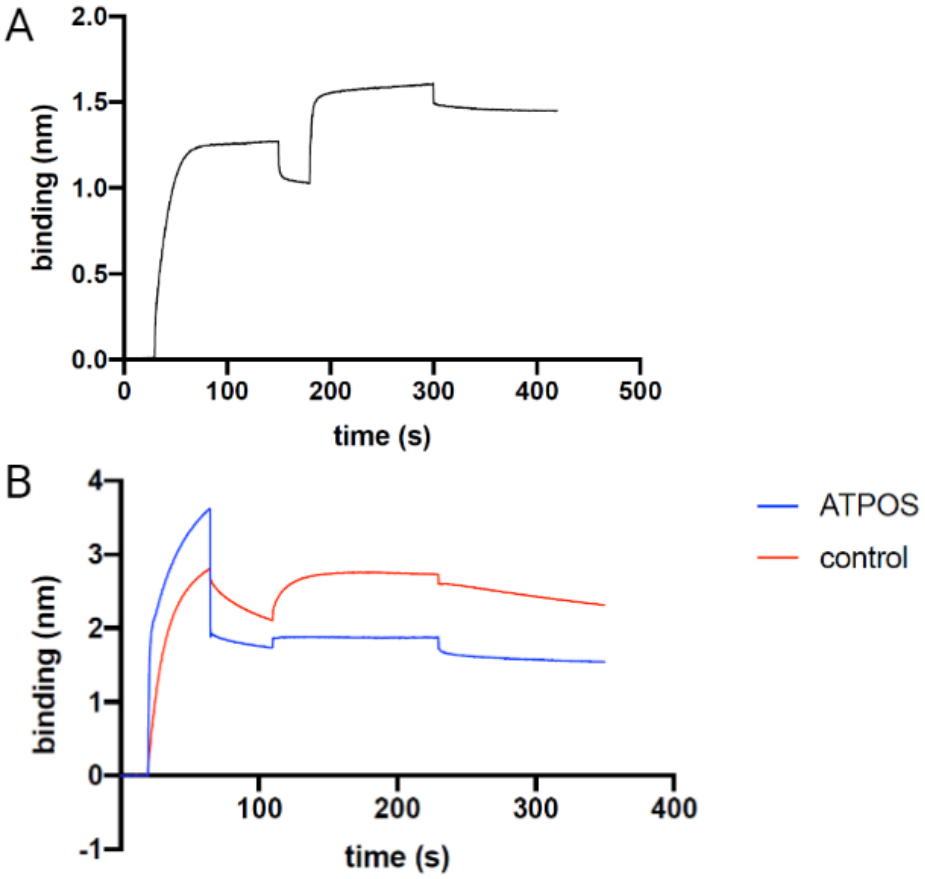

Figure 20 Analysis of ATPOS interactions using bio-layer interferometry. (A) Protein A biosensor was loaded with biotinylated ALFA Nb and incubated with ATPOS. No significant dissociation was detected, suggesting an efficient binding. (B) Protein A biosensor was loaded with biotinylated anti-cmyc Ab. Second baseline was measured and the sample was loaded. As positive control, a purified protein (construct 271 of Tobias Stähler from AG Nolte) containing cmyc tag was used (red line). Association was observed and no significant dissociation detected. A fresh biosensor was loaded with Ab and coated with ATPOS (blue line). No significant association occurred. During dissociation, the signal fell back to the level of the second baseline, suggesting weak to no binding.

detected in PE channel even in absence of ATP.

First, general binding experiments were performed without any sensor present. One approach was to couple soluble SA with biotinylated anti-CD3 antibody to cells such as human peripheral blood mononuclear cells (PBMCs) or Jurkat cells (data not shown). The SA were conjugated to a fluorochrome to monitor the success. After successful coating of the cells with SA, biotinylated cmyc antibody was added. B-cmyc binding

was detected via fluorescence detection of fluorochrome conjugated antibody against mouse IgG1. It only binds to b-cmyc (mouse IgG1 antibody) and does not recognize b-CD3 (mouse IgG2a antibody). Although b-cmyc binding was confirmed, no significant increase of the median PE-fluorescence intensity of cells was observed in flow cytometry analysis when ATPOS was present. Besides, binding analysis using bio-layer interferometry (BLI) showed no interaction between b-cmyc antibody and ATPOS. Degrading or contamination of the antibody solution could be excluded as an explanation for the lack of an increased signal due to binding of the positive control (see Fig. 20 B). AT-

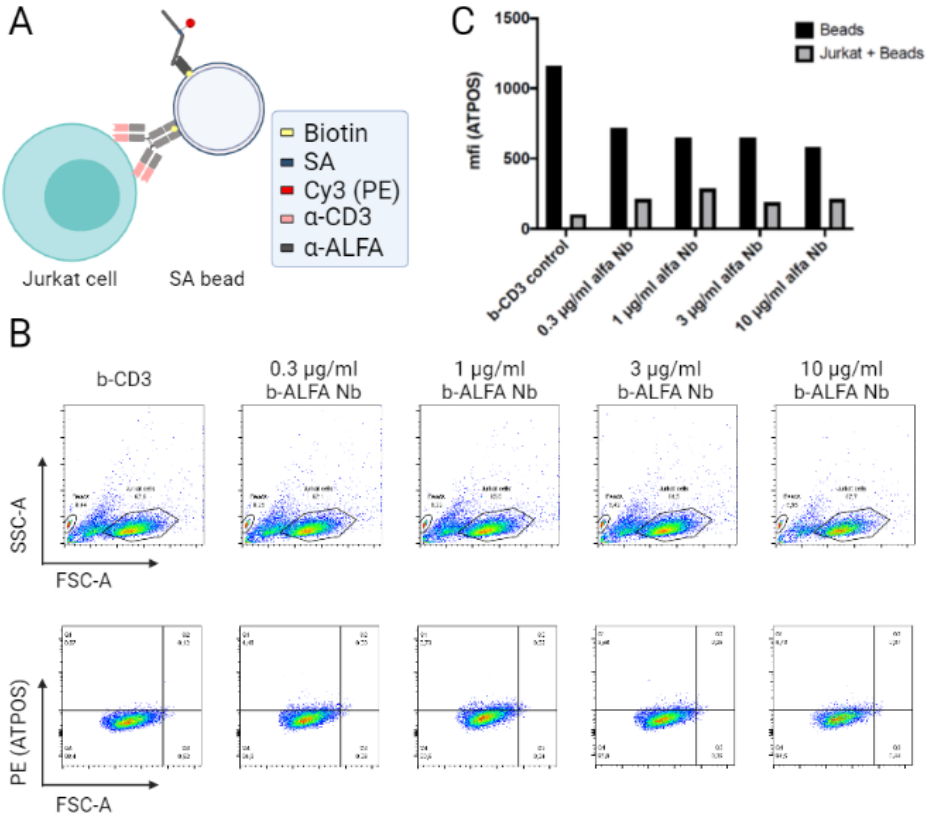

Figure 21 Titration of b-ALFA nanobody with beads. (A) SA coated beads were used to bring ATPOS close to the cell surface to measure local ATP concentrations. They were labelled with biotinylated anti-CD3 antibody and biotinylated ALFA nanobody which binds ATPOS. (B) The beads were labelled with Ab (1 μg/mL), Nb (0.3 - 10 μg/mL), incubated with ATPOS and added to the Jurkat cells. Flow cytometry was used for analysis. SSC was plotted against FSC to gate for Jurkat cells and free beads separately. Jurkat cell gate was further plotted, PE fluorescence against FSC. (C) Mfi of both gates was determined and plotted against Nb concentration. The free beads showed no significant change in mfi in presence of different Nb-Ab ratios while the gate with free cells and cell-bead complexes had the highest signal in presence of 1 μg/mL Nb. (A) was created with BioRender.com.

POS was constructed with another tag besides cmyc tag the ALFA tag. Therefore, binding of an anti-ALFA nanobody was tested with BLItz and showed strong binding (see Fig. 20 A). Biotinylated anti-ALFA nanobody was provided by Tobias Stähler of AG Nolte. In the following experiments, b-ALFA Nb was used instead of b-cmyc

antibody to bind ATPOS. Antibody, nanobody and sensor were titrated (shown with beads in Fig. 21) and in the following experiments 1 μg/mL b-CD3, 3 μg/mL nanobody and 16 μg/mL ATPOS were used.

Complex building was also tested with streptavidin coated transparent 5 μm beads instead of soluble SA. The beads were coated with b-CD3 antibody and b-ALFA nanobody (see Fig. 21). Figure 21 A describes the labeling schematically and Figure 21 B shows the formed complexes in dot plot. As control, beads coated with only b-CD3 were incubated with cells and ATPOS to check if large bead-cell complexes could be detected. As displayed in Figure 21 B, there are distinguished populations of free (unbound) beads and Jurkat cells. Some cell-bead complexes are possibly included in the Jurkat cell gate. Fluorescence signals for both gates are shown in Figure 21 C. Mfi of free beads was higher for all samples than fluorescence of the cell gate. Control showed with 1159 the highest value measured for unbound beads, while mfi of 102 was the lowest value measured for cells. The free bead's fluorescence decreased in presence of ALFA Nb. With 0.3 μg/mL b-ALFA Nb and 1 μg/mL b-CD3 Ab coated, mfi of 715 was measured. When coated with 1 μg/mL and 3 μg/mL Nb, mfi was almost the same with 649 and 648. Fluorescence decreased further to 586 when beads were coated with 10 μg/mL Nb. The mfi of the gated cells and cell-bead complexes was at 213 with

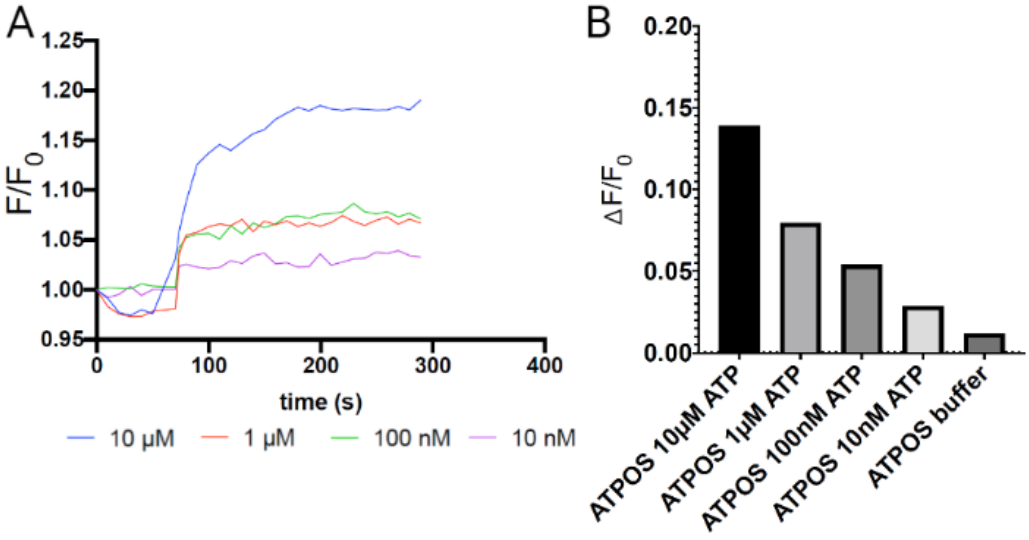

Figure 22 Responsiveness of ATPOS to ATP. ATP sensor function of ATPOS was evaluated in solution (in PBS) and analyzed with the plate reader at 575 nm. For this purpose, 21.6 μM ATPOS were used and different ATP concentrations (10 nM - 10 μM) were added. Fluorescence was detected over time. (A) F/F_0 is shown over time for four different ATP concentrations. The highest (10 μM, in blue) and the lowest (10 nM, in yellow) concentration also result in the highest and the lowest signal. Detected fluorescence in presence of 1 μM and 100 nM ATP shows no significant difference. (B) The fluorescence change, before to after addition, is shown for the individual ATP concentrations including the application of calcium buffer instead of ATP as control.

0.3 μg/mL Nb on the beads. It increased to 287 with beads coated with 1 μg/mL Nb

and showed a decrease to 188 with 3 μg/mL Nb. With 10 μg/mL Nb, almost the same signal (212) as with 0.3 μg/mL Nb (213) was reached.

5.2.3 ATP sensor function

ATPOS' responsiveness to ATP was tested in solution in cooperation with Valerie Brock from AG Guse. For this purpose, 21.6 μM sensor were used with different ATP concentrations (see Fig. 22). Base line was measured for 1 min before ATP was added. Figure 22 A describes the binding over time. ATPOS shows the highest signal in presence of the highest ATP concentration (10 μM) and lowest fluorescence at 10 nM ATP. The measured values fluctuated but showed a clear trend to saturation. The values for 1 μM and 100 nM were very close to each other and did not seem to be clearly distinguishable. In this cell-free system, ATPOS showed detectable response to ATP and its sensor function could be confirmed.

Confocal microscopy was used to prove the sensors activity when immobilized and

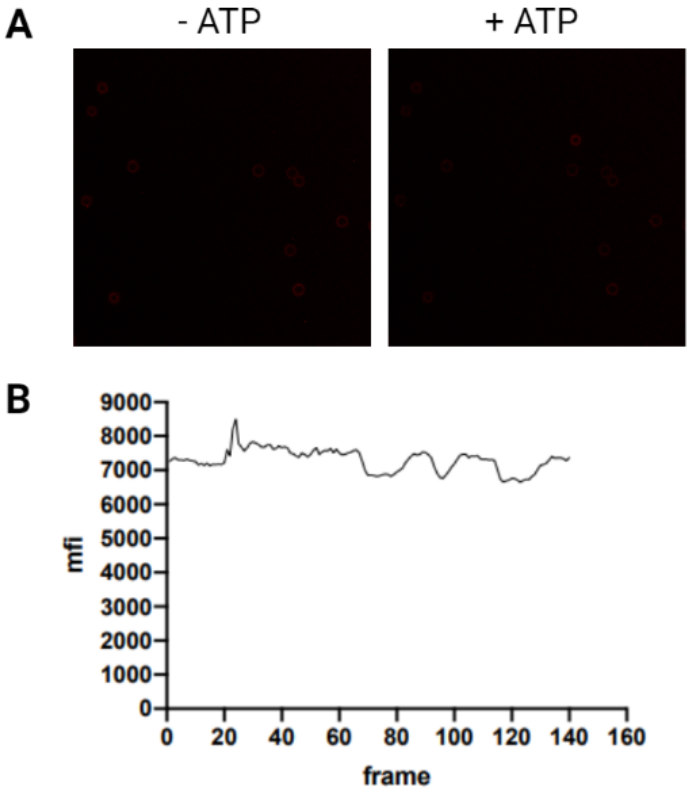

Figure 23 Analysis of ATPOS labeled beads using confocal microscopy. SA coated transparent 5 μm beads were labeled with biotinylated ALFA nanobody which binds ATPOS. (A) The left picture shows the beads before adding 160 μM ATP. The right picture shows the beads 3.5 min after ATP addition. (B) The mfi is plotted against the frame number. Each frame corresponds to one second. ATP was added after 30 s (frame 30). Microscopy was performed by Samantha Eiberg in cooperation with the UKE Microscopy Imaging Facility (umif).

bound to cells or beads. According to the binding experiments (see 4.3.5) SA coated transparent 5 μm beads were coated with b-CD3 Ab and ALFA Nb and then labeled

with ATPOS. Without cells, the beads were not fixed on the slide, causing floatation leading to impeding optimal detection, especially when ATP was added. Figure 23 A shows coated beads before and after ATP addition. There are no obvious changes in fluorescence except a single bead which was brighter than the others. As shown in Figure 23 B, the mfi fluctuates and no significant increase in fluorescence could be observed. The results were inconclusive. To prevent beads from floating in the following experiments, Jurkat cells were fixed on slides (see 4.3.5) and incubated with coated beads according to previous binding experiments (see Fig. 10). In the same experiment, Jurkat cells labeled with SA and ATPOS were used. Three different ATP concentrations were tested with cells and SA, but the results were alike. As shown in Figure 24 A, high basic fluorescence was measured before ATP was added. Meaning, bright red cells were visible without stimulation. Fluorescence did not change significantly after adding of ATP. Mfi seemed even to decrease after ATP addition (see Fig. 24 B).

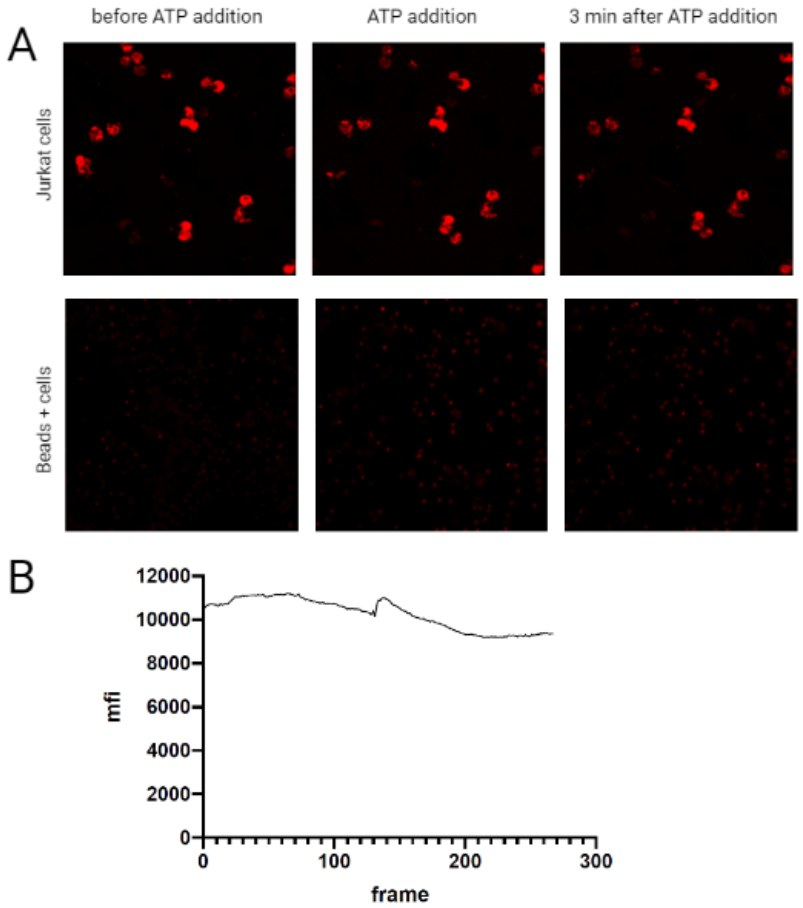

Figure 24 Analysis of ATPOS labeled Jurkat cells using confocal microscopy. (A) SA coated transparent 5 μm beads and soluble SA were both co-stained with biotinylated anti-CD3 antibody and biotinylated ALFA nanobody which binds ATPOS. The upper row shows Jurkat cells labeled with the SA-ATPOS complex before and after adding 160 μM ATP. The lower row shows Jurkat cells labeled with the bead-ATPOS complex before and after adding ATP. (B) The mfi is plotted against the frame number. Each frame corresponds to one second. ATP was added after 150 s (frame 150). Microscopy was performed by Samantha Eiberg in cooperation with the UKE Microscopy Imaging Facility (umif).

6 Discussion

The aim of this work was to construct sensor molecules for detection of extracellular ATP concentration levels. ATP plays an important role as energy carrier as well as extracellular signalling molecule. To understand the processes modulated by ATP it is important to be able to measure and quantify the changes of intra- and extracellular ATP. In this thesis, two single wavelength sensors were cloned, expressed, and purified. Both sensors were tested in solution and bound to cells and beads. In the following, the two sensors are compared with each other and set into context with the state of research.

Imamura *et al.* (2009) developed a FRET-based ATP sensor named ATeam. It is based on the ϵ-subunit of bacterial F0F1-ATP synthase from *Bacillus sp.* PS3 as ATP binding domain CFP. YFP were used as FRET pair. ATP binding induces a conformational change resulting in alteration of the distance between CFP and YFP. The FRET pair is exitated at 405 nm. In absence of ATP, fluorescence emission from the donor CFP at 475 nm is primary detected while YFP acceptor emission at 527 nm dominates in presence of ATP [37]. The three sensors used in this work are based on ATeam and were developed by Lobas *et al.* (2019) [42] and Kitajima *et al.* (2020) [41], respectively. They all have the same ATP binding domain - the ϵ-subunit of the F0F1-ATPase from *Bacillus* PS3. According to Lobas *et al.* (2019) and Kitajima *et al.* (2020), respectively, fluorescence increases as result of conformational change due to ATP binding. The sensor invented by Lobas *et al.* (2019) named iATPSnFr$^{1.1}$ (HHM1.1) contains a modified version of GFP (cpSFGFP) with the ATP binding domain cloned inside. HHM1.1 is used in this thesis as fusion protein with TP1170 nanobody, which recognizes and binds κ light chains of mouse antibodies. As negative control, a TP1170_HHM1.1 variant named TP1170_HHM1.1_RRKK was used. This variant contained two point mutations in its ATP binding domain to alter its ability to bind ATP. The third ATP sensor used in this thesis was developed by Kitajima *et al.* (2020). It is named ATPOS and has the same ATP binding domain as TP1170_HHM1.1. This binding domain is labelled with Cy3-maleimide. Its fluorescence increases as a result of ATP binding due to conformational changes.

6.1 Purification of ATP sensors

Lobas *et al.* (2019) and Kitajima *et al.* (2020) both used FPLC to purify their sensor constructs. In this work, TP1170_HHM1.1 and TP1170_HHM1.1_RRKK were purified using gravity flow instead of FPLC. Therefore, purity of the target protein was not as high as it was for ATPOS with FPLC at CSSB. Analysis with SDS-PAGE and western blot showed additional bands in both protein stock solutions, suggesting contamination. Using gravity flow columns, only a few (three to six) elution steps were performed

and all of them were pooled. ATPOS was purified with ÄKTA system. UV absorbance and conductivity were measured on the end of the column and signals were shown in a chromatogram. UV-peaks were an indicator for protein elution in general. Fractions containing just the target protein were combined and concentrated as shown in the chromatogram and SDS-PAGE analysis. Therefore, measured ATPOS' concentration can be assumed as real concentration of the ATP sensor. Due to detected contamination, concentration of TP1170_HHM1.1 and TP1170_HHM1.1_RRKK, respectively, may be lower than the measured value since total protein concentration was determined by NanoDrop or BCA test. TP1170_HHM1.1 and TP1170_HHM1.1_RRKK were purified with the same methods but protein yield was much higher for TP1170_HHM1.1. In ATP binding experiments, similar fluorescence signals were detected although concentration of the RRKK variant was 10 times lower. One possible explanation is that the measured concentration is incorrect. To compare the two sensor variants, the same concentration should be used in the experiments. Another explanation might be that the contamination in RRKK's stock solution was lower than in TP1170_HHM1.1's. If contamination was higher in one solution, it is harder to compare the two of them properly because only total protein concentration is measured.

6.2 Strategies to anchor the sensor to the cell surface

The aim of this work was to measure local ATP concentration close to the cell surface. Therefore, the ATP sensors had to be anchored in the cell membrane. Kitajima *et al.* (2020) used soluble SA labelled with Alexa 488 to bring ATPOS to neuronal cell membranes. SA was coated with biotinylated ATPOS and biotinylated BoNT/C-Hc which binds to gangliosides on the cell surface. In this work a similar approach was used. Here, ATPOS was not directly coupled to SA or SA coated transparent beads through biotinylation of the protein, but instead bound to a biotinylated antibody. In first experiments, a biotinylated anti-cmyc antibody was used to bind ATPOS to SA. Analysis with flow cytometry and BLItz showed no binding. One explanation for this is a loss of cmyc tag during expression, purification or modification. The tag is positioned on N terminus between NEDD8 domain and ALFA tag. NEDP1 protease should cleave specifically at NEDD8 domain but the tag might be damaged during cleavage. Binding could be tested before separating the His tag to rule out this possibility. It would also be possible to locate the cmyc tag C terminal and not N terminal. Another explanation could be that the protein formed multimers (presumably dimers), which leads to steric hinderance. To evaluate if multimerization could be prevented, different conditions of modification and storage could be tested. Since cmyc tag could not be used to link ATPOS to beads or SA, a biotinylated nanobody recognizing the sensor's N-terminal ALFA tag was used instead. Binding was confirmed with BLItz analysis.
Lobas *et al.* (2019) designed HHM1.1 to be expressed in the target cell (e.g. neurons)

and extracellularly displayed on plasma membrane, whereas TP1170_HHM1.1 and TP1170_HHM1.1_RRKK were both expressed in bacteria, purified, and used on human cells or beads. The nanobody was chosen as fusion partner to couple the sensor through a mouse antibody to the cell surface. TP1170 was developed by Pleiner *et al.* (2018) [45] to recognize and bind κ light chain of mouse antibodies. Jurkat cells or PBMCs were labelled with an appropriate antibody and stained with the sensor. Initial experiments did not show any clear results, as the chosen concentration was probably too low. Therefore, specific binding to mouse Ab could not be proven. Another approach was to label SA coated beads with the sensor via TwinStrep tag and bind this complex with biotinylated Ab to the cell surface. Flow cytometry analysis showed no significant increase in fluorescence intensity. This could be an indicator that the tag did not bind suffiently to SA. It is also possible that too much biotin was left after elution from Ni-TED column and following buffer exchange. In this case biotin would bind with higher affinity, preventing the sensor from binding. A new batch was produced, biotin was separated using Amicon column and binding was evaluated with BLItz analysis. Interaction between sensor and mouse antibody (b-cmyc) was detected and binding was proven. The same experiment with rat antibody showed no binding. Specific binding of TP1170_HHM1.1 to κ light chain mouse Ab was confirmed.

6.3 Validating ATP sensor function

TP1170_HHM1.1 and TP1170_HHM1.1_RRKK showed similar response to ATP. An increase of fluorescence was detected with the RRKK variant in presence of ATP contrary to its designed function. Its sequence was validated after cloning. Therefore, contamination might have been an issue, which effects fluorescence intensity. According to Lobas *et al.* (2019), fluorescence increases with higher ATP concentration between 1 μM and 1 mM. Dose-response curve for HHM1.1 was acquired with excitation at 488 nm and emission at 515 nm. For TP1170_HHM1.1, decrease in mfi was detected in presence of ATP. Fluorescence for TP1170_HHM1.1 was acquired with excitation at 485 nm and emission at 535 nm. TP1170_HHM1.1 and TP1170_HHM1.1_RRKK were only tested in a small range of ATP concentrations (1 - 50 μM). Further experiments with additional higher ATP concentrations would be necessary to be able to validate their function as ATP sensor. Lobas *et al.* (2019) also tested their sensors *in vitro* with cells using confocal microscopy. TP1170_HHM1.1 and TP1170_HHM1.1_RRKK were only tested in solution with ATP. A batch with higher purity could be tested with cells and analysed with microscopy. If there is a lot of contamination left, cells might be activated by the other bacterial proteins and ATP would be released. The sensor's response to certain ATP concentrations could not be detected under these conditions due to interferring signals because of released ATP.

Kitajima *et al.* (2020) described dose-response for ATPOS in solution with ATP con-

centrations between 1 nM and 10 μM. Fluorescence increase from F/F_0 of 1.0 to ca. 1.8. Dose-response curve for ATPOS was acquired with excitation at 556 nm and emission at 566 nm. In this work ATPOS was tested in solution with four different ATP concentrations between 10 nM and 10 µM. It was acquired with excitation at 545 nm and emission at 575 nm. Measurements with wavelenghts for excitation and emission as described by Kitajima *et al.*, resulted in overlapping spectra and high signals for all samples (including blank). Therefore, wavelenghts were adjusted. ATPOS' function in cell free system was confirmed. The sensor was also evaluated with confocal microscopy. Kitajima *et al.* (2020) labelled neurons with ATPOS-SA complex and detected Cy3, Alexa 488 and the ratio of them in absence or presence of ATP (200 nM and 20 μM). They showed a visible change in fluorescence ratio with ATP present to prove sensor function. In this work, confocal microscopy was used with transparent beads and Jurkat cells. Although the used SA was fluorochrome labelled (APC), no ratio was measured. The used fluorochrome could not be detected with this microscope. To detect fluorescence ratio between SA and ATPOS, another dye should be used for either SA or ATPOS. The initial experiments were performed with SA coated transparent beads labelled with ATPOS in presence (160 μM) and absence of ATP. No significant change in fluorescence intensity was observed. The same experiment in presence of immobilized Jurkat cells also showed no increase in mfi. The cells were not stained with any dye, so cell shape could not be detected. For further experiments, cells should be stained (e.g. with fluorochrome conjugated Abs against proteins expressed on the cell surface) when beads are used to bring ATPOS to the cell surface. SA-ATPOS complexes were also tested with immobilized Jurkat cells. The cells showed bright red signals unter the microscope without further stimulation. One possible explanation is that anti-CD3 was used to bring the ATPOS complex to the cell surface. Anti-CD3 antibody binding can activate T cells, resulting in ATP release. If ATP was already present when the measurement started, it is possible that fluorescence decreases over time when ATP is not bound anymore and degraded. In that case adding more ATP would not lead to increased fluorescence because saturation is already reached. Instead of anti-CD3, other antibodies such as anti-CD45 could be used to bind the ATPOS complex to the cell surface and anti-CD3 could be used to stimulate the cell. Fluorescence ratio of SA to ATPOS could also provide more information about subsequently released ATP.

7 Conclusion and Outlook

In this work three ATP sensor constructs were cloned, expressed and purified. Purification success was higher for ATPOS than for the other two due to the use of FPLC system. TP1170_HHM1.1 and TP1170_HHM1.1_RRKK still showed contaminations in SDS-PAGE analysis after purification. Therefore, FPLC should be used instead of gravity flow if possible. All constructs could be successfully linked to the cell surface. TP1170_HHM1.1 and TP1170_HHM1.1_RRKK bound to mouse antibody labelled cells directly via TP1170 nanobody. Therefore, specific binding was proven. ATPOS was successfully coupled to cell surface via fluorochrome conjugated soluble SA and SA coated transparent beads, respectively, co-labelled with biotinylated anti-CD3 antibody and biotinylated anti-ALFA nanobody. Sensor function was validated for ATPOS in solution while TP1170_HHM1.1 and TP1170_HHM1.1_RRKK have to be further investigated. For ATPOS a RRKK variant was cloned but has to be expressed, purified and modified for further experiments. Response-dose curves of all four sensor constructs to ATP could be measured to determine their sensitivity. In this work, only the response to ATP was evaluated. Other nucleotides and ATP metabolites such as ADP should be tested as well to prove selectivity for ATP. Binding kinetics could be determined according to Kitajima *et al.* (2020). It would be also important to know if ATP binding is reversible. This could be achieved with measurements over time with and without reagents to degrade ATP.

8 Abstract

Adenosine triphosphate (ATP) is known as the universal energy carrier of living cells. In addition, ATP plays an important role as a paracrine and autocrine signalling molecule. The release of ATP is involved in many biological processes such as the regulation of the immune system and inflammatory responses, but ATP also has an important function as a neurotransmitter. Since the ATP concentrations relevant for these processes are in the nanomolar range at the cell surface, measuring them is a technical challenge. The luciferin-luciferase system is the most used assay for measuring ATP concentrations. However, only global concentration changes are detected. The small molecule ATP sensors used in this work are recruited to the cell surface and immobilized there, making it possible to detect local ATP concentrations by live cell imaging. The aim of the work was to construct fluorescent sensor molecules for the detection of local concentrations of extracellular ATP. For this purpose, first the ordered sequences of the GFP-based sensors TP1170_HHM1.1 and TP1170_HHM1.1_RRKK, as well as of ATPOS, were cloned, expressed in bacteria and finally purified. ATPOS was coupled with the dye Cy3 via a maleimide bond. Different strategies were followed to bring the sensor molecules to the cell surface. The two GFP-based sensors are fusion proteins from the ATP sensor iATPSnFR$^{1.1}$ (HHM1.1) constructed by Lobas *et al.* (2019) and the TP1170 nanobody developed by Pleiner *et al.*
TP1170 specifically binds the κ light chain of mouse antibodies. To couple TP1170_HHM1.1 or TP1170_HHM1.1_RRKK to the cell membrane, cells were coated with mouse antibodies recognized by TP1170. To bring the ATPOS sensor developed by Kitajima *et al.* (2020) close to the cell surface, the sensors were bound to streptavidin-coated beads via a biotinylated nanobody directed against ATPOS' ALFA tag. The beads were also loaded with an antibody directed against a cell surface antigen. Flow cytometry and confocal microscopy confirmed the coupling of sensor and cell and bead, respectively. The function as an ATP sensor could be demonstrated for ATPOS in solution. For the validation of TP1170_HHM1.1 and TP1170_HHM1.1_RRKK further investigation is necessary. Further engineering of these sensors will allow measurement of physiologically relevant concentrations of ATP and visualization of ATP release from target cells, like activated immune cells.

9 Zusammenfassung

Adenosintriphosphat (ATP) ist als universeller Energieträger lebender Zellen bekannt. Zudem spielt ATP eine wichtige Rolle als parakrines und autokrines Signalmolekül. Die Freisetzung von ATP ist an vielen biologischen Prozessen wie der Regulation des Immunsystems und von Entzündungsreaktionen beteiligt, aber auch als Neurotransmitter hat ATP eine wichtige Funktion. Da die für diese Prozesse relevanten ATP-Konzentrationen an der Zelloberfläche im nanomolaren Bereich liegen, stellt ihre Messung allerdings eine technische Herausforderung dar. Das Luziferin-Luziferase-System ist das am weitesten verbreitete Assay zur Bestimmung von ATP-Konzentrationen. Jedoch werden dabei nur globale Konzentrationsänderungen detektiert. Die in dieser Arbeit verwendeten niedermolekularen ATP-Sensoren werden an die Zelloberfläche gebracht und dort immobilisiert, wodurch es möglich ist, lokale ATP-Konzentrationen mittels Live-Cell-Imaging zu detektieren.

Ziel der Arbeit war die Konstruktion fluoreszierender Sensormoleküle zur Detektion lokaler Konzentrationen von extrazellulärem ATP. Dazu wurden zunächst die bestellten Sequenzen der GFP basierten Sensoren TP1170_HHM1.1 und TP1170_HHM1.1_RRKK, sowie von ATPOS kloniert, in Bakterien exprimiert und schließlich aufgereinigt. ATPOS wurde mit dem Farbstoff Cy3 über eine Maleimidbindung gekoppelt.

Um die Sensormoleküle an die Zelloberfläche zu bringen, wurden verschiedene Strategien verfolgt. Die beiden GFP basierten Sensoren sind Fusionsproteine aus dem von Lobas *et al.* (2019) konstruierten ATP-Sensor iATPSnFR$^{1.1}$ (HHM1.1) und dem von Pleiner *et al.* entwickelten TP1170 Nanobody. TP1170 bindet spezifisch die κ leichte Kette von Mausantikörpern. Um TP1170_HHM1.1 bzw. TP1170_HHM1.1_RRKK an die Zellmembran zu koppeln, wurden die Zellen mit Mausantikörpern beschichtet, die von TP1170 erkannt wurden.

Um den von Kitajima *et al.* (2020) entwickelten Sensor ATPOS in die Nähe der Zelloberfläche zu bringen, wurde der Sensor über einen biotinylierten, gegen ATPOS' ALFA Tag gerichteten, Nanobody an Streptavidin-beschichtete Beads gebunden, die zusätzlich mit einem gegen ein Zelloberflächenantigen gerichteten Antikörper beladen waren. Durchflusszytometrie und konfokale Mikroskopie bestätigten die Kopplung von Sensor und Zelle bzw. Bead. Die Funktion als ATP-Sensor konnte für ATPOS in Lösung nachgewiesen werden. Zur Validierung von TP1170_HHM1.1 und TP1170_HHM1.1_RRKK sind noch weitere Untersuchen notwendig. Die Weiterentwicklung dieser Sensoren wird künftig die Messung physiologisch relevanter ATP-Konzentrationen und somit auch die Visualisierung der ATP-Freisetzung von Zielzellen wie aktivierten Immunzellen ermöglichen.

References

1. Bours, M. J. L., Swennen, E. L. R., Di Virgilio, F., Cronstein, B. N. & Dagnelie, P. C. Adenosine 5'-triphosphate and adenosine as endogenous signaling molecules in immunity and inflammation. eng. *Pharmacology & therapeutics* **112.** Journal Article Review, 358 404. ISSN: 0163-7258. eprint: 16784779 (2006).
2. Berg, J. M., Tymoczko, J. L., Stryer, L. & Gatto, G. J. *Biochemie* 7. Auflage. ger. Berg, Jeremy M. (VerfasserIn) Tymoczko, John L. (VerfasserIn) Stryer, Lubert (VerfasserIn) Gatto, Gregory J. (VerfasserIn) Held, Andreas (ÜbersetzerIn) Held, Manuela (ÜbersetzerIn) Jarosch, Birgit (ÜbersetzerIn) Maxam, Gudrun (ÜbersetzerIn) Seidler, Lothar (ÜbersetzerIn). 1196 pp. ISBN: 978-3-8274-2988-9 (Springer Spektrum, Berlin and Heidelberg, 2013).
3. Knowles, J. R. Enzyme-catalyzed phosphoryl transfer reactions. eng. *Annual review of biochemistry* **49.** Journal Article Research Support, U.S. Gov't, Non-P.H.S. Research Support, U.S. Gov't, P.H.S. Review, 877 919. ISSN: 0066-4154. eprint: 6250450 (1980).
4. Burnstock, G. Purinergic nerves. eng. *Pharmacological reviews* **24.** Journal Article Review, 509 581. ISSN: 0031-6997. eprint: 4404211 (1972).
5. Burnstock, G., Cocks, T., Kasakov, L. & Wong, H. K. Direct evidence for ATP release from non-adrenergic, non-cholinergic ("purinergic") nerves in the guinea-pig taenia coli and bladder. *European journal of pharmacology* **49.** PII: 0014299978900705, 145 149 (1978).
6. Corriden, R. & Insel, P. A. Basal release of ATP: an autocrine-paracrine mechanism for cell regulation. eng. *Science signaling* **3.** Journal Article Review, re1. eprint: 20068232 (2010).
7. Coade, S. B. & Pearson, J. D. Metabolism of adenine nucleotides in human blood. eng. *Circulation research* **65.** Journal Article, 531 537. ISSN: 0009-7330. eprint: 2548757 (1989).
8. Forrester, T. An estimate of adenosine triphosphate release into the venous effluent from exercising human forearm muscle. eng. *The Journal of physiology* **224.** Journal Article, 611 628. ISSN: 0022-3751. eprint: 5071932 (1972).
9. Beis, I. & Newsholme, E. A. The contents of adenine nucleotides, phosphagens and some glycolytic intermediates in resting muscles from vertebrates and invertebrates. eng. *The Biochemical journal* **152.** Comparative Study Journal Article, 23 32. ISSN: 0264-6021. eprint: 1212224 (1975).
10. Trautmann, A. Extracellular ATP in the immune system: more than just a "danger signal". eng. *Science signaling* **2.** Journal Article Review, pe6. eprint: 19193605 (2009).
11. Pellegatti, P. *et al.* Increased level of extracellular ATP at tumor sites: in vivo imaging with plasma membrane luciferase. eng. *PloS one* **3.** Evaluation Study Journal Article Research Support, Non-U.S. Gov't, e2599. eprint: 18612415 (2008).
12. Milo, R., Jorgensen, P., Moran, U., Weber, G. & Springer, M. BioNumbers the database of key numbers in molecular and cell biology. eng. *Nucleic acids research* **38.** Journal Article Research Support, Non-U.S. Gov't, D750 3. eprint: 19854939 (2010).

13. Campwala, H. & Fountain, S. J. Constitutive and agonist stimulated ATP secretion in leukocytes. eng. *Communicative & integrative biology* **6.** Journal Article, e23631. ISSN: 1942-0889. eprint: 23713132 (2013).

14. Yegutkin, G. G. Nucleotide- and nucleoside-converting ectoenzymes: Important modulators of purinergic signalling cascade. eng. *Biochimica et biophysica acta* **1783.** Journal Article Research Support, Non-U.S. Gov't Review, 673 694. ISSN: 0006-3002. eprint: 18302942 (2008).

15. Praetorius, H. A. & Leipziger, J. ATP release from non-excitable cells. eng. *Purinergic signalling* **5.** Journal Article, 433 446. eprint: 19301146 (2009).

16. Elliott, M. R. *et al.* Nucleotides released by apoptotic cells act as a find-me signal to promote phagocytic clearance. eng. *Nature* **461.** Journal Article Research Support, N.I.H., Extramural Research Support, Non-U.S. Gov't, 282 286. eprint: 19741708 (2009).

17. Antonioli, L., Pacher, P., Vizi, E. S. & Haskó, G. CD39 and CD73 in immunity and inflammation. eng. *Trends in molecular medicine* **19.** Journal Article Research Support, N.I.H., Extramural Research Support, U.S. Gov't, Non-P.H.S. Review, 355 367. eprint: 23601906 (2013).

18. Lazarowski, E. R., Boucher, R. C. & Harden, T. K. Constitutive release of ATP and evidence for major contribution of ecto-nucleotide pyrophosphatase and nucleoside diphosphokinase to extracellular nucleotide concentrations. eng. *The Journal of biological chemistry* **275.** Journal Article Research Support, Non-U.S. Gov't Research Support, U.S. Gov't, P.H.S., 31061 31068. ISSN: 0021-9258. eprint: 10913128 (2000).

19. Murphy, K. M. & Weaver, C. *Janeway's immunobiology* 9th edition. eng. In collab. with Mowat, A. *et al.* Murphy, Kenneth M. (VerfasserIn) Weaver, Casey (VerfasserIn) Mowat, Allan (MitwirkendeR) Berg, Leslie (MitwirkendeR) Chaplin, David (MitwirkendeR) Janeway, Charles (MitwirkendeR) Travers, Paul (MitwirkendeR) Walport, Mark (MitwirkendeR). 904 pp. ISBN: 978-0-8153-4505-3 (GS Garland Science Taylor & Francis Group, New York and London, 2017).

20. Fitz, J. G. Regulation of cellular ATP release. eng. *Transactions of the American Clinical and Climatological Association* **118.** Journal Article Review, 199 208. ISSN: 0065-7778. eprint: 18528503 (2007).

21. Klaus Eric Kaschubowski. *Use of fluorescent sensors to visualize P2X7-mediated changes in local ATP concentrations in the cytosol and at the cell surface* (2020).

22. Vitiello, L., Gorini, S., Rosano, G. & La Sala, A. Immunoregulation through extracellular nucleotides. eng. *Blood* **120.** Journal Article Research Support, Non-U.S. Gov't, 511 518. eprint: 22661701 (2012).

23. Lotfi, R. *et al.* ATP promotes immunosuppressive capacities of mesenchymal stromal cells by enhancing the expression of indoleamine dioxygenase. eng. *Immunity, inflammation and disease* **6.** Journal Article Research Support, Non-U.S. Gov't, 448 455. eprint: 30306723 (2018).

24. Di Virgilio, F., Boeynaems, J.-M. & Robson, S. C. Extracellular nucleotides as negative modulators of immunity. eng. *Current opinion in pharmacology* **9.** Journal Article Research Support, Non-U.S. Gov't Review, 507 513. eprint: 19628431 (2009).

25. Burnstock, G. Purine and pyrimidine receptors. eng. *Cellular and molecular life sciences : CMLS* **64.** Journal Article Review, 1471 1483. ISSN: 1420-682X. eprint: 17375261 (2007).

26. Kumar, V. & Sharma, A. Adenosine: an endogenous modulator of innate immune system with therapeutic potential. eng. *European journal of pharmacology* **616.** Journal Article Review, 7 15. eprint: 19464286 (2009).

27. Haskó, G., Csóka, B., Németh, Z. H., Vizi, E. S. & Pacher, P. A(2B) adenosine receptors in immunity and inflammation. eng. *Trends in immunology* **30.** Journal Article Research Support, N.I.H., Extramural Research Support, N.I.H., Intramural Research Support, Non-U.S. Gov't Review, 263 270. eprint: 19427267 (2009).

28. Stagg, J. & Smyth, M. J. Extracellular adenosine triphosphate and adenosine in cancer. eng. *Oncogene* **29.** Journal Article Research Support, Non-U.S. Gov't Review, 5346 5358. eprint: 20661219 (2010).

29. DeLuca, M. & McElroy, W. D. Kinetics of the firefly luciferase catalyzed reactions. eng. *Biochemistry* **13.** Journal Article, 921 925. ISSN: 0006-2960. eprint: 4813372 (1974).

30. Singhal, P. & Kuhr, W. G. Direct electrochemical detection of purine- and pyrimidine-based nucleotides with sinusoidal voltammetry. eng. *Analytical chemistry* **69.** Journal Article, 3552 3557. ISSN: 0003-2700. eprint: 21639279 (1997).

31. Kueng, A., Kranz, C. & Mizaikoff, B. Amperometric ATP biosensor based on polymer entrapped enzymes. eng. *Biosensors & bioelectronics* **19.** Journal Article Research Support, Non-U.S. Gov't Research Support, U.S. Gov't, Non-P.H.S., 1301 1307. ISSN: 0956-5663. eprint: 15046763 (2004).

32. Llaudet, E., Hatz, S., Droniou, M. & Dale, N. Microelectrode biosensor for real-time measurement of ATP in biological tissue. eng. *Analytical chemistry* **77.** Journal Article Research Support, Non-U.S. Gov't, 3267 3273. ISSN: 0003-2700. eprint: 15889918 (2005).

33. Brown, P. & Dale, N. Spike-independent release of ATP from Xenopus spinal neurons evoked by activation of glutamate receptors. eng. *The Journal of physiology* **540.** Journal Article Research Support, Non-U.S. Gov't, 851 860. ISSN: 0022-3751. eprint: 11986374 (2002).

34. Pangršič, T. *et al.* Exocytotic release of ATP from cultured astrocytes. eng. *The Journal of biological chemistry* **282.** Journal Article Research Support, Non-U.S. Gov't, 28749 28758. ISSN: 0021-9258. eprint: 17627942 (2007).

35. Anselmi, F. *et al.* ATP release through connexin hemichannels and gap junction transfer of second messengers propagate Ca2+ signals across the inner ear. eng. *Proceedings of the National Academy of Sciences of the United States of America* **105.** Journal Article Research Support, N.I.H., Extramural Research Support, Non-U.S. Gov't, 18770 18775. eprint: 19047635 (2008).

36. Huang, Y.-J. *et al.* The role of pannexin 1 hemichannels in ATP release and cell-cell communication in mouse taste buds. eng. *Proceedings of the National Academy of Sciences of the United States of America* **104.** Comparative Study Journal Article Research Support, N.I.H., Extramural, 6436 6441. eprint: 17389364 (2007).

37. Imamura, H. *et al.* Visualization of ATP levels inside single living cells with fluorescence resonance energy transfer-based genetically encoded indicators. eng. *Proceedings of the National Academy of Sciences of the United States of America* **106.** Journal Article Research Support, Non-U.S. Gov't, 15651 15656. eprint: 19720993 (2009).

38. Yaginuma, H. *et al.* Diversity in ATP concentrations in a single bacterial cell population revealed by quantitative single-cell imaging. eng. *Scientific reports* **4.** Journal Article Research Support, Non-U.S. Gov't, 6522. eprint: 25283467 (2014).

39. Shrestha, D., Jenei, A., Nagy, P., Vereb, G. & Szöllősi, J. Understanding FRET as a research tool for cellular studies. eng. *International journal of molecular sciences* **16.** Journal Article Research Support, Non-U.S. Gov't Review, 6718 6756. eprint: 25815593 (2015).

40. Lindenburg, L. & Merkx, M. Engineering genetically encoded FRET sensors. eng. *Sensors (Basel, Switzerland)* **14.** Journal Article Research Support, Non-U.S. Gov't, 11691 11713. eprint: 24991940 (2014).

41. Kitajima, N. *et al.* Real-time in vivo imaging of extracellular ATP in the brain with a hybrid-type fluorescent sensor. eng. *eLife* **9.** Journal Article Research Support, Non-U.S. Gov't NK, KT, HS, KS, DA, HS, ST, KH, YU, SN, MI, KH No competing interests declared. eprint: 32648544 (2020).

42. Lobas, M. A. *et al.* A genetically encoded single-wavelength sensor for imaging cytosolic and cell surface ATP. eng. *Nature communications* **10.** Journal Article Research Support, N.I.H., Extramural Research Support, Non-U.S. Gov't, 711. eprint: 30755613 (2019).

43. Abbas, A. K., Lichtman, A. H., Pillai, S. & Baker, D. L. *Cellular and molecular immunology. Study smart with student consult ; studentconsult.com* 8. ed., internat. ed. eng. 535 pp. ISBN: 978-0-323-22275-4 (Elsevier Saunders, Philadelphia, Pa., 2015).

44. Wesolowski, J. *et al.* Single domain antibodies: promising experimental and therapeutic tools in infection and immunity. eng. *Medical microbiology and immunology* **198.** Journal Article Research Support, Non-U.S. Gov't Review, 157 174. eprint: 19529959 (2009).

45. Pleiner, T., Bates, M. & Görlich, D. A toolbox of anti-mouse and anti-rabbit IgG secondary nanobodies. eng. *The Journal of cell biology* **217.** Journal Article Research Support, Non-U.S. Gov't, 1143 1154. eprint: 29263082 (2018).

46. Rahbarizadeh, F., Ahmadvand, D. & Sharifzadeh, Z. Nanobody; an old concept and new vehicle for immunotargeting. eng. *Immunological investigations* **40.** Journal Article Review, 299 338. eprint: 21244216 (2011).

47. Deffar, K., Shi, H., Wang, X. & Zhu, X. Nanobodies - the new concept in antibody engineering. *African Journal of Biotechnology,* 2645 2652. https://doi.org/10.5897/AJB09.353 (2009).

48. Shiz Aoki. *BioRender* 2021. https://app.biorender.com/biorender-templates.

Appendix

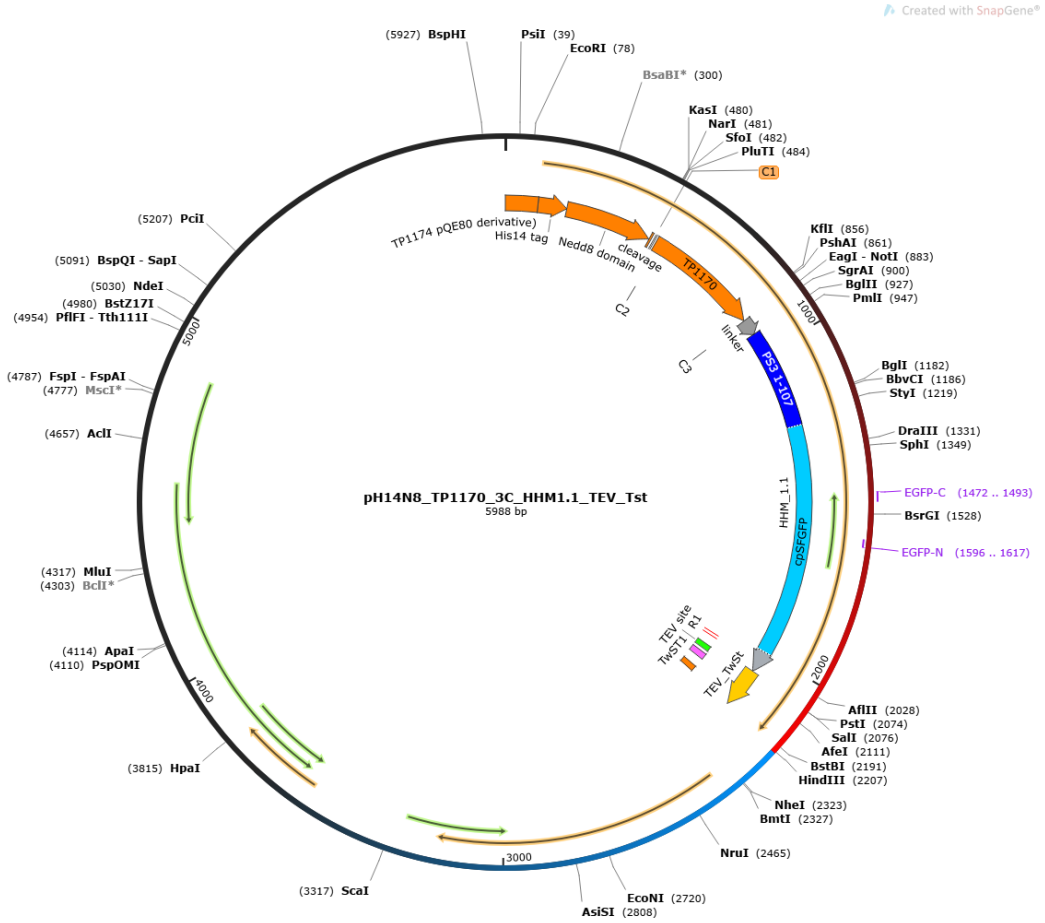

Figure 25 Gene map pH14N8_TP1170_3C_HHM1.1_TEV_Tst. Created with Snap Gene.

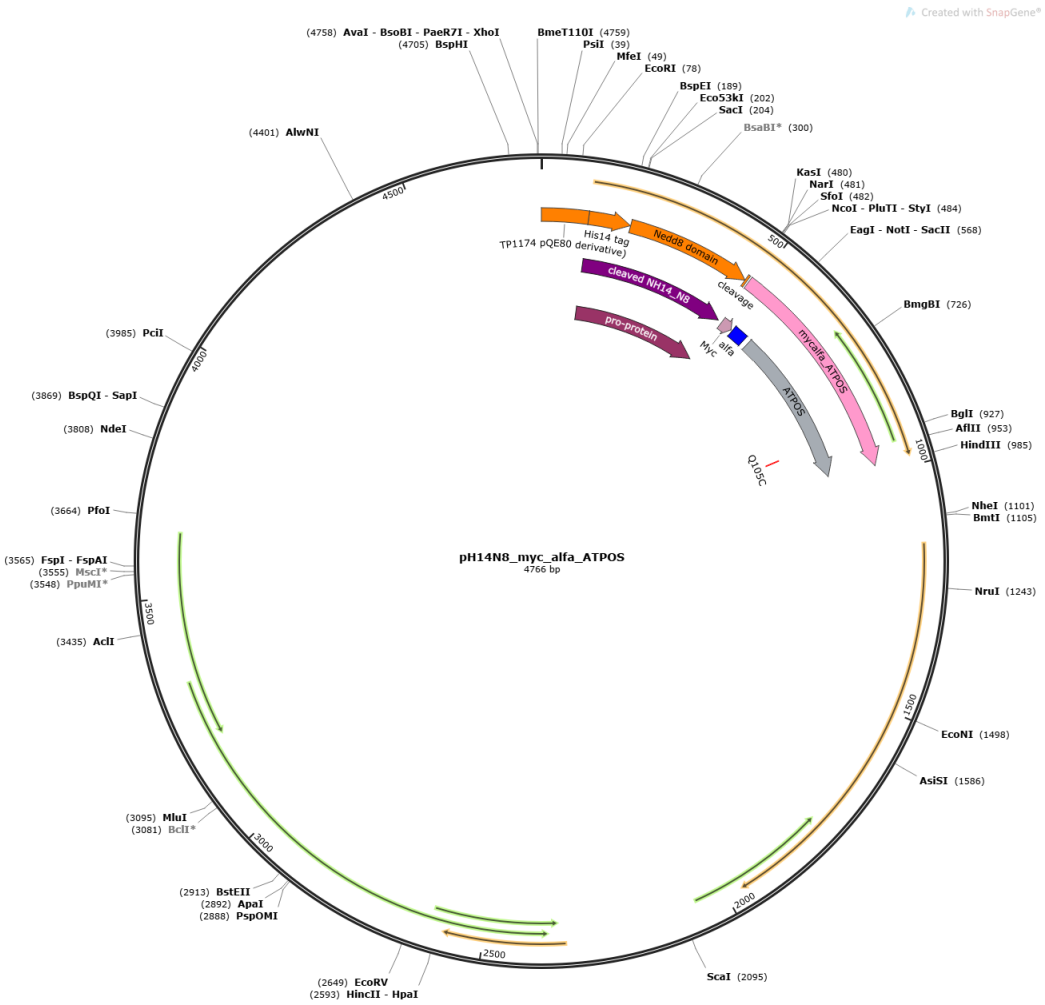

Figure 26 Gene map pH14N8_myc_alfa_ATPOS. Created with Snap Gene.

Table 14 Overview digested inserts

1) TP1170_HHM1.1	
1x NEB buffer 2.1	2 μl
HHM1.1	16 μl
Not I	1 μl
Hind III	1 μl
Total	20 μl

2) TP1170_HHM1.1_RRKK	
1x NEB buffer 2.1	2 μl
HHM1.1_RRKK	16 μl
Not I	1 μl
Hind III	1 μl
Total	20 μl

3) cmyc_alfa_ATPOS	
1x NEB buffer 2.1	2 μl
ATPOS	16 μl
Kas I	1 μl
Hind III	1 μl
Total	20 μl

4) 3) cmyc_alfa_ATPOS_RRKK	
1x NEB buffer 2.1	2 μl
ATPOS_RRKK	16 μl
Not I	1 μl
Hind III	1 μl
Total	20 μl

Table 15 Overview digested vectors

1) pH14N8_TP1170_3C_TEV_TwST	
1x NEB buffer 2.1	2 µl
vector	12 µl
Not I	1 µl
Hind III	1 µl
ddH_2O	4 µl
Total	20 µl

2) pH14N8_TP1170_3C_HHM1.1_TEV_TwST	
1x NEB buffer 2.1	2 µl
vector	2,2 µl
Kas I	1 µl
Hind III	1 µl
ddH_2O	13,8 µl
Total	20 µl

Eidesstattliche Erklärung

Ich versichere, die von mir vorgelegte Arbeit selbstständig verfasst zu haben. Alle Stellen, die wörtlich oder sinngemäß aus veröffentlichten oder nicht veröffentlichten Arbeiten anderer entnommen sind, habe ich als entnommen kenntlich gemacht. Sämtliche Quellen und Hilfsmittel, die ich für die Arbeit benutzt habe, sind angegeben. Die Arbeit hat mit gleichem Inhalt bzw. in wesentlichen Teilen noch keiner anderen Prüfungsbehörde vorgelegen.

$Unterschrift$: $Ort, Datum$: